Summer 8-15-2018

Noninvasive Multi-Modality Studies of Cardiac Electrophysiology, Mechanics, and Anatomical Substrate in Healthy Adults, Arrhythmogenic Cardiomyopathy, and Heart Failure

Christopher Andrews
Washington University in St. Louis

WASHINGTON UNIVERSITY IN ST. LOUIS

School of Engineering & Applied Sciences

Department of Biomedical Engineering

Dissertation Examination Committee:
Yoram Rudy, Chair
Mitchell N. Faddis
Jonathan R. Silva
Gautam K. Singh
Pamela K. Woodard

Noninvasive Multi-Modality Studies of Cardiac Electrophysiology, Mechanics, and Anatomical Substrate in Healthy Adults, Arrhythmogenic Cardiomyopathy, and Heart Failure

by

Christopher Andrews

A dissertation presented to
The Graduate School
of Washington University in
partial fulfillment of the
requirements for the degree
of Doctor of Philosophy

August 2018
St. Louis, Missouri

Table of Contents

List of Figures

List of Tables

Acknowledgments

I would like to thank my advisor, Yoram Rudy, for his guidance and support. I would like to thank the members of the Rudy lab, especially Ramya Vijayakumar and Junjie Zhang, for their helpful discussions about our research. I would also like to thank our clinical collaborators: Phil Cuculich, Scott Marrus, Dan Cooper, and Jen Silva for their help along the way. I would like to thank Julia Meyer for her assistance with control patient data collection and Nicole Joison for her contribution to the tagged MRI analysis. I would like to thank the co-authors of the studies in this thesis. And finally, I would like to thank to my wife, Amanda, and our families for their support during my PhD.

This study was supported by NIH – National Heart, Lung and Blood Institute grants R01-HL-033343 and R01-HL-049054 (to YR) and by Washington University Institute of Clinical and Translational Sciences grant UL1-TR000448 from the National Center for Advancing Translational Sciences of the NIH.

Christopher Andrews

Washington University in St. Louis

August 2018

This thesis is dedicated to the patients who participated in these studies.

ABSTRACT OF THE DISSERTATION

Noninvasive Multi-Modality Studies of Cardiac Electrophysiology, Mechanics, and Anatomical Substrate in Healthy Adults, Arrhythmogenic Cardiomyopathy, and Heart Failure

by

Christopher Andrews

Doctor of Philosophy in Biomedical Engineering

Washington University in St. Louis, 2018

Professor Yoram Rudy, Chair

Heart disease is a leading cause of death and disability and is a major contributor to healthcare costs. Many forms of heart disease are caused by abnormalities in the electrical function of heart muscle cells or the cardiac conduction system. Electrocardiographic Imaging (ECGI) is a noninvasive modality for imaging cardiac electrophysiology. By combining recordings of the voltage distribution on the torso surface with anatomical images of the heart-torso geometry, ECGI reconstructs voltages on the epicardium. This thesis applies ECGI to novel studies of human heart function and disease and explores new combinations of ECGI with additional imaging modalities.

ECGI was applied in combination with late gadolinium enhancement (LGE) scar imaging MRI in patients with arrhythmogenic right ventricular cardiomyopathy (ARVC). ARVC carries a high risk of sudden cardiac death, and the hallmark feature of ARVC is the progressive replacement of healthy myocardium with fibrous and fatty tissue. By combining ECGI and LGE in ARVC patients we found that there are signs of conduction abnormalities before structural abnormalities can be detected in ARVC patients. Electrical and structural abnormalities in ARVC patients co-

localized. We also found that PVCs, potential triggers for arrhythmia, originated in regions of structural and electrical abnormalities.

ECGI was applied in combination with speckle tracking echocardiography (STE) to longitudinally image heart failure patients undergoing cardiac resynchronization therapy (CRT). STE is an echocardiographic technique for measuring strain (contraction) in the heart. CRT is a highly effective treatment for heart failure, however, around 30% of patients do not respond to the treatment. ECGI was more effective for predicting response to CRT than the current standard ECG criteria or STE indices. The timing of peak contraction in STE did not accurately reflect the electrical activation sequence. CRT caused improvements in contraction that persisted even when pacing was disabled. CRT prolonged repolarization at the site of the LV pacing lead, which may increase the risk of arrhythmia in CRT patients.

The above studies contribute novel observations of human disease physiology and demonstrate the clinical feasibility and effectiveness of ECGI for noninvasive assessment of ARVC and CRT.

Chapter 1: Introduction

1.1 Heart Disease and Electrophysiology

Heart disease is a leading cause of death and disability and is a major contributor to healthcare costs [1]. The pumping function of the heart is controlled by synchronized contractions of heart muscle cells called cardiomyocytes. Cardiomyocyte contractions are controlled by changes to the voltage gradient across the cell membrane. The characteristic membrane voltage signal associated with cardiomyocyte contraction is called the cardiac action potential. The first phase of the action potential is an increase in membrane voltage known as depolarization. Depolarization begins the process of cardiomyocyte contraction through a process known as excitation-contraction coupling. The membrane voltage remains elevated and contraction continues through the plateau phase of the action potentials. Finally, the membrane voltage returns to resting levels and contraction ends due to a process known as repolarization. All phases of the cardiac action potential are controlled by a delicate balance of ionic current flow through specialized transmembrane proteins known as ion channels. In order for the heart to pump blood efficiently, heart muscle cells must contract synchronously. Synchronization of cardiomyocyte contractions is accomplished by a specialized conduction system within the heart and electrical coupling between adjacent cells. When cardiomyocyte action potentials are coordinated by this cardiac conduction system, the collective action potentials of all contracting cells result in a voltage signal that can be measured from the body surface.

1.1.1 Electrocardiogram (ECG)

Recordings of the electrical activity associated with cardiac contraction were first made in the 1800s. The characteristic voltage signal on the body surface was named the "electrocardiogram" (abbreviated ECG or EKG, interchangeably) by Willem Einthoven, who won the Nobel prize in 1924 for his research on the ECG [2]. While the electronics for recording the ECG have improved considerably (Einthoven's ECG recording apparatus weighed over 600 pounds), ECG recordings have evolved very little over the past 50 years. The current standard of practice is the 12-lead ECG, which records the cardiac electrical activity from standardized locations on the chest and limbs.

1.1.2 ECG Abnormalities and Arrhythmia

Many forms of heart disease are associated with ECG abnormalities. Alterations to any aspect of the conduction system in the heart or the cardiac action potential can lead to abnormal ECG findings. There are many mechanisms that cause these alterations, including structural damage caused by heart attacks, genetic mutations that affect ion channels or other important structures, and progressive heart diseases. Alterations to the normal ECG rhythm are known as arrhythmias and range in severity from benign to imminently life-threatening. The most important diagnostic tool for arrhythmias is the ECG.

1.2 Electrocardiographic Imaging

ECG recordings from the body-surface reflect the electrical activity of the entire heart, with regions close to the recording electrodes having a larger contribution to the signal than more distant regions. While the ECG is massively important to clinical cardiology, its resolution is limited by the distance of the electrodes from the heart surface. Electrocardiographic Imaging

(ECGI) is a novel imaging technique that greatly improves upon the resolution of the standard 12-lead ECG. ECGI is performed by solving the inverse problem in electrocardiography.

1.2.1 Theoretical Background

The inverse problem is governed by Laplace's equation ($\nabla^2\Phi = 0$) and boundary equations on the heart and torso surfaces [3]. In plain terms, Laplace's equation describes the relationship between voltages on an inner surface (the heart) and an outer surface (the torso). Laplace's equation can be applied to the heart-torso geometry when there are no electrical sources between the heart and torso surfaces. When Laplace's equation holds, it is possible to apply boundary conditions to calculate the value of the voltage on one of the surfaces when the position of the inner surface relative to the outer surface is known. Solutions to Laplace's equation for arbitrary geometries can be formulated by discretizing the inner and outer surfaces and solving the equation with the Boundary Element Method [4]. Therefore, applying Laplace's equation the heart requires the position of the heart relative to the torso surface and knowledge of the boundary conditions.

The first boundary condition applied to Laplace's equation in ECGI states that the normal derivative of voltage is zero at the torso surface. This condition holds because the air surrounding the torso is an insulating medium that does not support current flow out of the body. The second boundary condition is that the voltage on the heart surface is known. Applying these conditions and solving for the voltage on the torso-surface is known as the forward problem in electrocardiography. However, ECGI is concerned with the inverse problem in electrocardiography. To solve for the inverse problem, the terms of the forward problem are rearranged to formulate an equation for the voltage on the surface of the heart as a function of the

voltage on the torso surface, which can be easily measured non-invasively. While a unique solution to the inverse problem exists, the inverse problem is "ill-posed."

The term ill-posed means that small inaccuracies in the measurements of the input values may produce very large errors in the output. Sources of inaccuracy in the electrocardiographic inverse problem include noise in voltage measurements and small inaccuracies introduced by representing the heart-torso geometry using discretized surfaces. Because these sources of noise are unavoidable, regularization is employed to stabilize the solutions to the inverse problem. The term regularization broadly encompasses various strategies that have been developed to stabilize the solutions to ill-posed problems [5-10].

1.2.2 Methodology

ECGI is performed by combining ECG recordings from the torso of patients with non-invasive imaging of the heart-torso geometry, then computing voltages on the heart by applying regularization to the inverse problem. A schematic of the procedure is presented in **Figure 1.1**. Approximately 250 ECGs are simultaneously recorded from the torso-surface. After the recordings are obtained, patients are imaged using a computed tomography (CT) or magnetic resonance imaging (MRI) scan to obtain images of the heart-torso geometry. A novel contribution of this thesis was a modification of the imaging protocol to enable compatibility with MRI. Compatibility is achieved by removing the electrode strips, which cannot be safely worn in the magnetic field of an MRI scanner, and replacing them with MRI-visible marker strips. This process is depicted in **Figure 1.2**. A major benefit of this modification is that it avoids exposing patients to the ionizing radiation of a CT scan.

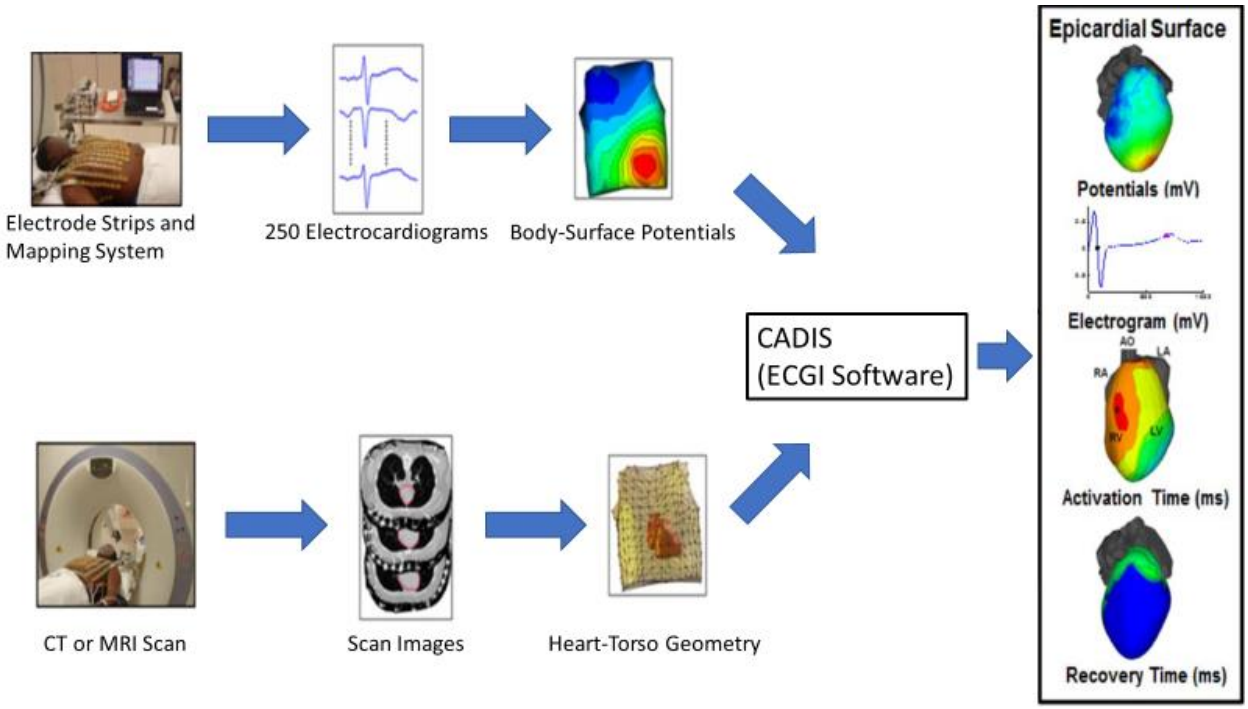

Figure 1.1 Schematic of the ECGI procedure. Body-surface potentials are recorded from the torso surface using a portable recording system (top). The heart-torso geometry is obtained using a computed tomography (CT) or magnetic resonance imaging (MRI) scan (bottom). The heart-torso geometry and torso potentials are combined and the inverse problem is solved to reconstruct unipolar epicardial electrograms. Electrograms are processed to determine local electrical parameters of interest (right frame).

1.2.3 Validation

The methodology of ECGI has been developed and extensively validated over multiple decades. The technique was first validated using tank-torso studies. In these studies, animal hearts were suspended in a human torso-shaped tank, and reconstructed voltages on the heart surface (referred to as electrograms) were validated using directly-measured values [11]. ECGI reconstructions were also validated in humans by comparing reconstructed electrograms to direct intraoperative mapping recordings [12]. After many years of incremental improvements to the technique and validation, the current implementation has been successfully applied to many studies of human arrhythmia [13-15].

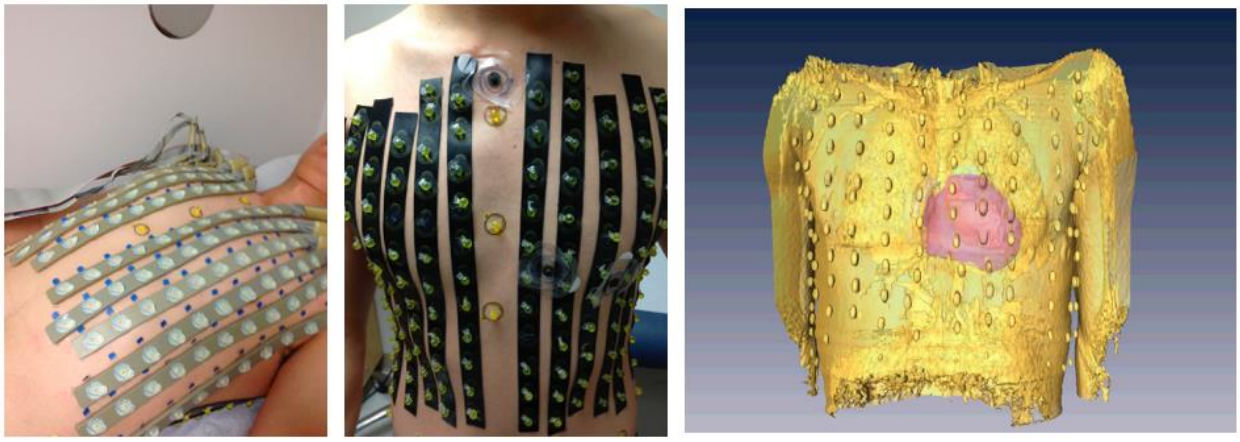

Figure 1.2 Modification to the Electrocardiographic Imaging (ECGI) procedure for MRI compatibility. Recording electrodes (left) cannot be safely worn in the magnetic field of an MRI scanner. The electrodes are removed and replaced with strips of MRI-visible markers (middle). The resulting images reveal the position of the electrodes relative to the heart surface (right), which is necessary for the ECGI reconstruction.

1.3 Dissertation Organization

Chapters 2 and 3 of this thesis describe novel applications of ECGI. In each case, ECGI is combined with additional noninvasive imaging techniques to study clinically important diseases. A common thread of each of these studies, and a significant contribution of this thesis, is a population of healthy adult controls. As ECGI is applied to additional forms of heart disease, a control group of healthy adults is increasingly important. In each of the co-authored chapters that follow, my role was to serve as the individual primarily responsible for data collection, analysis, and manuscript preparation. The motivation and experimental techniques applied in Chapters 2 and 3 are described below. Chapter 4 concludes this thesis with remarks about the overall contributions of these research efforts and future research directions that can build on the work presented here.

1.4 Overview of Chapter 2

1.4.1 Study Design

Chapter 2 is an investigation of ECGI and structural imaging in 20 patients diagnosed with arrhythmogenic right ventricular cardiomyopathy (ARVC). This study was performed in collaboration with researchers at University College London. In this study, ARVC patients were imaged with ECGI and late gadolinium enhancement (LGE) MRI. Patients in this study also exercised using a supine bicycle. In many patients the exercise induced premature ventricular contractions (PVCs), which are potential triggers of arrhythmia. We mapped the location of the PVCs using ECGI and related the PVCs to structural and electrical abnormalities.

1.4.2 Arrhythmogenic Right Ventricular Cardiomyopathy (ARVC)

ARVC is a major cause of sudden death in young individuals and has a prevalence estimated as high as 1 in 1000 [16]. The disease was originally called arrhythmogenic right ventricular dysplasia (ARVD) because it was thought to be caused by a congenital defect in the right ventricle. However, we now know the disease is caused by genetic defects in desmosomes, which are the structures that connect cardiomyocytes [17]. Desmosomal mutations progressively cause the distinctive feature of ARVC, which is a loss of healthy heart muscle (myocardium) and replacement by fibrous and fatty tissue [17]. This progressive process of fibrofatty tissue replacement is thought to cause abnormal conduction of the electrical signal for contraction, which can lead to dangerous arrhythmias. The risk of sudden death in patients with ARVC may be increased by sports activity. The rarity and progressive nature of ARVC make diagnosis and risk stratification extremely difficult. In many cases, the first manifestation of ARVC is sudden cardiac death. The only treatment proven to prevent sudden death is implantable cardioverter

defibrillator (ICD) implantation, however, implantation carries risks and primary prevention indications remain a matter of debate [18,19]. Because the key feature of ARVC is fibrofatty tissue replacement, structural imaging techniques appear well-suited to for application to ARVC. However, the regions of scar in ARVC may be small and diffuse, making them difficult to detect with conventional imaging techniques. There is also evidence that the earliest signs of the disease are electrical abnormalities.

1.4.3 Late Gadolinium Enhancement

Late gadolinium enhancement (LGE) is an imaging technique that can detect evidence of structural scar in the heart [20]. LGE imaging is performed by injecting patients with an MRI-visible contrast agent. Regions of tissue with increased extracellular space (e.g., regions of cardiac scar) accumulate more of the contrast agent and appear brighter when imaged [21].

1.4.4 Key Findings

We found abnormal conduction and repolarization in ARVC patients compared to controls. These abnormalities spatially co-localized with structural scar imaged with LGE. The majority of patients had PVCs, which generally increased in frequency during exercise. The PVCs originated in regions of electrical abnormalities and structural scar, making these regions a good target for clinical intervention. ECGI detected conduction abnormalities in a young patient with ARVC who had no other physical symptoms and no visible scar in LGE.

1.5 Overview of Chapter 3

1.5.1 Study Design

Chapter 3 is a prospective longitudinal study of heart failure in 30 patients undergoing cardiac resynchronization therapy (CRT). Patients were imaged using ECGI and speckle-tracking echocardiography (STE) prior to treatment, which allowed us to test how well the imaging techniques were able to predict favorable response to treatment. We performed repeat imaging after 3 and 6 months of treatment to observe how the heart physiology changes in response to CRT. In addition to performing ECGI and STE in a control group of 20 healthy patients, we performed tagged MRI on the controls.

1.5.2 Heart Failure and Cardiac Resynchronization Therapy (CRT)

In contrast to ARVC, which is relatively rare, heart failure is highly prevalent. An estimated 6.5 million American adults have heart failure, and this number is projected to grow to more than 8 million by 2030 [1]. While the 5-year fatality rate after hospitalization for heart failure is still very high at 42.3%, it represents a substantial improvement thanks to continued advances in treatment [1]. One of the most significant advances in the treatment of heart failure is cardiac resynchronization therapy (CRT). CRT is a pacemaker-based treatment that is designed to improve the synchrony of contractions in the heart. Approximately 30% of heart failure patients have regions of delayed electrical depolarization in their ventricles [22]. The result of this delay is that the contractions of the ventricles are not synchronized and do not pump blood as efficiently as normal, synchronized contractions. This electrical delay manifests in the portion of the ECG representing ventricular depolarization (known as the QRS complex) being wider than normal. CRT is effective at correcting some of this dyssynchrony by pacing the heart at multiple

locations to resynchronize contractions. Large-scale clinical trials have shown that CRT improves patient quality of life, reduces heart failure related hospitalizations, and prolongs patient survival [23-26]. While CRT has revolutionized treatment, it has been plagued by a remarkably stable rate of about 30% of patients who do not respond to the treatment. Because the dyssynchronous contraction in these patients is ultimately a mechanical phenomenon, there has been debate over whether mechanical imaging techniques can measure the dyssynchronous contractions and provide better patient selection criteria than the current ECG-based techniques.

1.5.3 Speckle-Tracking Echocardiography

Speckle-tracking echocardiography (STE) is an ultrasound-based imaging technique for measuring strain. Strain is a mechanical property defined as a change in a material's length divided by its original length. Strain is useful in cardiology as a measure of the contraction of heart muscle. Negative strain values indicate that the muscle contracted, while positive values indicate that it stretched. STE measures strain in cardiac ultrasound images by tracking characteristic speckled patterns that appear in these images and measuring the distances between those patterns. STE is most commonly performed in 2D views of the heart. Key advantages of STE include its high framerate and its safety in patients with implanted metal devices such as pacemakers.

1.5.4 Tagged MRI

Tagged MRI is an MRI-based technique for imaging strain and is considered a gold standard for measuring strain. Tagged MRI works by creating grid-shaped patterns in images of the heart, then tracking the motion of the grids over time. Key advantages of tagged MRI over STE are that

it provides full 3D strain in the entire left ventricle and that the grid features are not affected by their motion relative to the imaging plane.

1.5.5 Key Findings

The most effective predictor of response to CRT was the ventricular dyssynchrony measured with ECGI. The time of peak contraction measured by STE did not accurately reflect the electrical activation sequence, indicating that the strain curves are affected by other mechanical factors such as opposing wall contractions and do not always reflect the sequence of electrical activation. CRT caused beneficial improvements in contraction that persist even when pacing is disabled. CRT also caused prolonged repolarization in the area of the left ventricular pacing lead, which may increase the risk of arrhythmia in these patients.

Chapter 1 References

1. Benjamin EJ, Virani SS, Callaway CW, Chamberlain AM, Chang AR, Cheng S, Chiuve SE, Cushman M, Delling FN, Deo R, de Ferranti SD, Ferguson JF, Fornage M, Gillespie C, Isasi CR, Jiménez MC, Jordan LC, Judd SE, Lackland D, Lichtman JH, Lisabeth L, Liu S, Longenecker CT, Lutsey PL, Mackey JS, Matchar DB, Matsushita K, Mussolino ME, Nasir K, O'Flaherty M, Palaniappan LP, Pandey A, Pandey DK, Reeves MJ, Ritchey MD, Rodriguez CJ, Roth GA, Rosamond WD, Sampson UKA, Satou GM, Shah SH, Spartano NL, Tirschwell DL, Tsao CW, Voeks JH, Willey JZ, Wilkins JT, Wu JH, Alger HM, Wong SS, Muntner P. Heart Disease and Stroke Statistics—2018 Update: A Report From the American Heart Association. *Circulation*. 2018;137:e67–e492.

2. AlGhatrif M, Lindsay J. A brief review: history to understand fundamentals of electrocardiography. *Journal of Community Hospital Internal Medicine Perspectives*. 2012;2:14383.

3. Rudy Y, Messinger-Rapport BJ. The inverse problem in electrocardiography: solutions in terms of epicardial potentials. *Critical reviews in biomedical engineering*. 1988;16:215–268.

4. Hall WS. The Boundary Element Method (Solid Mechanics and Its Applications). 1st ed. Springer; 1993.

5. Hansen P, O'LEARY D. The use of the L-Curve in the regularization of discrete ill-posed problems. *SIAM J. Sci Comput*. 1993;14,6:1487-1503.

6. Messinger-Rapport BJ, Rudy Y. Computational issues of importance to the inverse recovery of epicardial potentials in a realistic heart-torso geometry. *Mathematical biosciences*. 1989;97:85–120.

7. Ramanathan C, Jia P, Ghanem R, Calvetti D, Rudy Y. Noninvasive electrocardiographic imaging (ECGI): application of the generalized minimal residual (GMRes) method. *Annals of biomedical engineering*. 2003;31:981–994.

8. Calvetti D, Lewis B, Reichel L. GMRES, L-curves, and discrete ill-posed problems. *BIT Numerical Mathematics*. 2002;

9. Saad Y, Schultz M. GMRES: A generalized minimal residual algorithm for solving nonsymmetric linear systems. *SIAM J Sci Stat Comput*. 1986;

10. Ghosh S, Rudy Y. Application of L1-norm regularization to epicardial potential solution of the inverse electrocardiography problem. *Annals of biomedical engineering*. 2009;37:902–912.

11. Messinger-Rapport BJ, Rudy Y. Noninvasive recovery of epicardial potentials in a realistic heart-torso geometry. Normal sinus rhythm. *Circ Res*. 1990;66:1023–1039.

12. Ghanem RN, Jia P, Ramanathan C, Ryu K, Markowitz A, Rudy Y. Noninvasive electrocardiographic imaging (ECGI): comparison to intraoperative mapping in patients. *Heart Rhythm*. 2005;2:339–354.

13. Zhang J, Sacher F, Hoffmayer K, O'Hara T, Strom M, Cuculich P, Silva J, Cooper D, Faddis M, Hocini M, Haïssaguerre M, Scheinman M, Rudy Y. Cardiac electrophysiological substrate underlying the ECG phenotype and electrogram abnormalities in Brugada syndrome patients. *Circulation*. 2015;131:1950–1959.

14. Vijayakumar R, Silva JNA, Desouza KA, Abraham RL, Strom M, Sacher F, Van Hare GF, Haïssaguerre M, Roden DM, Rudy Y. Electrophysiologic substrate in congenital Long QT syndrome: noninvasive mapping with electrocardiographic imaging (ECGI). *Circulation*. 2014;130:1936–1943.

15. Ramanathan C, Ghanem RN, Jia P, Ryu K, Rudy Y. Noninvasive electrocardiographic imaging for cardiac electrophysiology and arrhythmia. *Nat Med*. 2004;10:422–428.

16. Sen-Chowdhry S, Morgan RD, Chambers JC, McKenna WJ. Arrhythmogenic cardiomyopathy: etiology, diagnosis, and treatment. *Annu Rev Med*. 2010;61:233–253.

17. Arrhythmogenic Right Ventricular Cardiomyopathy. *N Engl J Med*. 2017;376:1489–1490.

18. Corrado D, Wichter T, Link MS, Hauer RNW, Marchlinski FE, Anastasakis A, Bauce B, Basso C, Brunckhorst C, Tsatsopoulou A, Tandri H, Paul M, Schmied C, Pelliccia A, Duru F, Protonotarios N, Estes NM, McKenna WJ, Thiene G, Marcus FI, Calkins H. Treatment of Arrhythmogenic Right Ventricular Cardiomyopathy/Dysplasia: An International Task Force Consensus Statement. American Heart Association Journals; 2015. p. 441–453.

19. Zorzi A, Rigato I, Bauce B, Pilichou K, Basso C, Thiene G, Iliceto S, Corrado D. Arrhythmogenic Right Ventricular Cardiomyopathy: Risk Stratification and Indications for Defibrillator Therapy. *Curr Cardiol Rep*. 2016;18:57–11.

20. Kellman P, Arai AE. Cardiac imaging techniques for physicians: late enhancement. *J Magn Reson Imaging*. 2012;36:529–542.

21. Doltra A. Emerging Concepts for Myocardial Late Gadolinium Enhancement MRI. *Current Cardiology Reviews*. 2013;9:185–190.

22. Kashani A, Barold SS. Significance of QRS complex duration in patients with heart failure. *J Am Coll Cardiol*. 2005;46:2183–2192.

23. Cleland JGF, Daubert J-C, Erdmann E, Freemantle N, Gras D, Kappenberger L, Tavazzi L, Cardiac Resynchronization-Heart Failure CARE-HF Study Investigators. The effect of cardiac resynchronization on morbidity and mortality in heart failure. *N Engl J Med*. 2005;352:1539–1549.

24. Abraham WT, Fisher WG, Smith AL, DeLurgio DB, Leon AR, Loh E, Kocovic DZ, Packer M, Clavell AL, Hayes DL, Ellestad M, Trupp RJ, Underwood J, Pickering F, Truex C, McAtee P, Messenger J, MIRACLE Study Group Multicenter InSync Randomized Clinical Evaluation. Cardiac resynchronization in chronic heart failure. *N Engl J Med*. 2002;346:1845–1853.

25. Bristow MR, Saxon LA, Boehmer J, Krueger S, Kass DA, de Marco T, Carson P, DiCarlo L, DeMets D, White BG, DeVries DW, Feldman AM, Comparison of Medical Therapy Pacing and Defibrillation in Heart Failure COMPANION Investigators. Cardiac-resynchronization therapy with or without an implantable defibrillator in advanced chronic heart failure. *N Engl J Med*. 2004;350:2140–2150.

26. Cleland JGF, Daubert J-C, Erdmann E, Freemantle N, Gras D, Kappenberger L, Tavazzi L. Longer-term effects of cardiac resynchronization therapy on mortality in heart failure [the CArdiac REsynchronization-Heart Failure (CARE-HF) trial extension phase]. *European heart journal*. 2006;27:1928–1932.

Chapter 2: The Electrical and Structural Substrate of Arrhythmogenic Right Ventricular Cardiomyopathy Determined Using Noninvasive Electrocardiographic Imaging and Late Gadolinium Magnetic Resonance Imaging

Circulation Arrhythmia and Electrophysiology. 2017;10:e005105.

Christopher M Andrews (BS), Neil T Srinivasan (MD), Stefania Rosmini (MD), Heerajnarain Bulluck (MD), Michele Orini (PhD), Sharon Jenkins (BSc), Antonis Pantazis (MD), William J McKenna (MD DSc), James C Moon (MD), Pier D Lambiase (MD PhD), and Yoram Rudy (PhD)

2.1 Abstract

Background: Arrhythmogenic right ventricular cardiomyopathy (ARVC) is a significant cause of sudden cardiac death in the young. Improved noninvasive assessment of ARVC and better understanding of the disease substrate are important for improving patient outcomes.

Methods and Results: We studied 20 genotyped ARVC patients with a broad spectrum of disease using Electrocardiographic Imaging (ECGI; a method for noninvasive cardiac electrophysiology (EP) mapping) and advanced late gadolinium enhancement (LGE) cardiac magnetic resonance scar imaging. Compared to 20 healthy controls, ARVC patients had longer ventricular activation duration (median 52 vs 42 ms; $p = 0.007$) and prolonged mean epicardial activation-recovery intervals (a surrogate for local action potential duration; median 275 vs 241 ms; $p = 0.014$). In these patients, we observed abnormal and varied epicardial activation breakthrough locations, and regions of non-uniform conduction and fractionated electrograms. Non-uniform conduction and fractionated electrograms were present in the early concealed phase of ARVC. EP abnormalities co-localized with LGE scar, indicating a relationship with structural disease. Premature ventricular contractions (PVCs) were common in ARVC patients with variable initiation sites in both ventricles. PVC rate increased with exercise, and within anatomical segments it correlated with prolonged repolarization, electrical markers of scar, and LGE (all $p < 0.001$).

Conclusions: ECGI reveals EP substrate properties that differ in ARVC patients compared to healthy controls. A novel mechanistic finding is the presence of repolarization abnormalities in regions where ventricular ectopy originates. The results suggest a potential role for ECGI and LGE in early diagnosis and non-invasive follow-up of ARVC patients.

2.2 Introduction

Arrhythmogenic right ventricular cardiomyopathy (ARVC) [abbreviations are defined in **Supplemental Table S2.1**] is an important hereditary cause of sudden cardiac death in young individuals with an estimated prevalence as high as 1:1000 [1,2]. The ARVC phenotype is progressive, consisting of an early concealed phase, overt arrhythmias, and heart failure. However, penetrance is variable and the first manifestation of the disease may be sudden cardiac death [1,2]. Diagnosis and treatment of ARVC are challenging, with implications for family screening and risk stratification [3,4].

ARVC is characterized by fibro-fatty infiltration of the myocardium with an epicardial predominance, suggesting that the disease progresses from epicardium to endocardium [5]. Fibro-fatty replacement in ARVC results from desmosomal mutations that lead to progressive cardiomyocyte death [6]. The desmosomal mutations cause decreased function of sodium channels and gap junctions in cardiomyocytes [6,7]. Exercise hastens disease progression by elevating myocardial wall stress, especially in the right ventricle (RV) [8], and has been linked to episodes of sudden cardiac death. Human and murine studies demonstrated that electrophysiological changes precede the structural disease [9]. Though originally described as a RV disease, there is increasing evidence for non-classical presentation with both biventricular and left ventricular (LV)-dominant disease [10].

Definitive diagnosis of ARVC requires histological demonstration of fibrofatty replacement of myocardium or the presence of a known ARVC genotype. Biopsy is challenging because the fibro-fatty infiltration may be patchy and epicardial. Genotypes linked to ARVC are present in only 30-40% of cases. Current diagnosis utilizes a combination of structural, functional, and

electrophysiological (EP) criteria [3]. However, diagnosis is challenging because of the progressive nature of ARVC and its early concealed phase. The only treatment proven to prevent sudden cardiac death in ARVC patients is the implantable cardioverter defibrillator (ICD). However, ICD implantation carries risks, and primary prevention indications remain a matter of debate [4,11].

Effective non-invasive modalities and improved understanding of ARVC arrhythmia mechanisms are essential for accurate diagnosis and risk stratification. As stated in a recent editorial, access to the epicardium for electrical measurements can enhance earlier disease detection. However, direct epicardial access is challenging and limited to experienced clinical centers [12]. The present study employs a noninvasive method (Electrocardiographic Imaging: ECGI; also referred to as Electrocardiographic Mapping (ECM) or body-surface mapping) [13] for epicardial EP mapping and the latest generation of magnetic resonance imaging (MRI) for cardiac structure (cardiac MRI (CMR) with advanced late gadolinium enhancement (LGE) using motion correction reconstruction) [14]. We applied ECGI and LGE to study the electrical and structural substrates in ARVC patients. These two techniques are safe, noninvasive, and well suited to longitudinal assessment of ARVC patients. The goal of this study is to provide insight into the myocardial substrate and arrhythmia mechanisms in ARVC. It also constitutes a preliminary exploration of the suitability of combined ECGI and LGE for diagnosis and risk stratification of ARVC patients.

2.3 Methods

2.3.1 Patient Cohort

Twenty ARVC patients with a broad spectrum of structural and electrophysiological disease were enrolled at the Heart Hospital, UCLH, London, UK. All patients were genotyped for

desmosomal mutations. Patient characteristics are summarized in **Table 2.1** (additional clinical characteristics provided in **Supplemental Tables S2.2 and S2.3**). The study was approved by the National Research Ethics Service Committee London (14/LO/0360) and the Human Research Protection Office at Washington University in St. Louis. All patients provided written informed consent. The study conformed to the declaration of Helsinki.

Table 2.1

Patient ID	Age	Gender	Mutation	Major Criteria	Minor Criteria
1	59	M	JUP	1	1
2	63	M	PKP2	1	3
3	54	F	PKP2	2	3
4	44	M	DSP	1	3
5	55	M	DSP	1	5
6	63	M	PKP2	3	3
7	59	M	DSP	1	3
8	69	F	PKP2	0	2
9	61	M	DSP	1	2
10	41	F	DSP*	1	1
11	49	F	PKP2	3	2
12	60	M	DSG	3	2
13	26	M	PKP2	0	3
14	66	M	PKP2	2	1
15	54	M	PKP2	2	0
16	74	M	DSG	1	3
17	24	M	DSP	1	0
18	54	M	Negative	2	2
19	39	M	Negative	2	2
20	75	M	Negative	2	3

ARVC patient characteristics including Task Force Major and Minor Criteria (numbers indicate how many Major and Minor Criteria were observed). Mutation abbreviations: Plakoglobin (JUP), Plakophilin-2 (PKP2), Desmoplakin (DSP), Desmoglein (DSG). Asterisk indicates variant of unknown significance.

2.3.2 ECGI and MRI

The ECGI method was developed and validated in our laboratory and described previously [13]. A schematic of the procedure is presented in **Supplemental Figure S2.1**. Briefly, 256 uniformly distributed body-surface electrocardiograms (ECGs) were recorded simultaneously using a portable recording system (ActiveTwo, BioSemi, Netherlands). Patients exercised on a supine ergometer for two minutes, followed by a ramp protocol of fifteen Watts/minute to a maximum heart rate (HR) of 120 beats/minute. Recordings were performed in the supine position at rest, during exercise, and immediately following exercise cessation. ECGI data were transferred to the Rudy lab for data processing, map construction, and analysis.

Following the recording protocol, CMR was performed in a 1.5 T scanner (Magnetom Avanto, Siemens Medical Solutions, Germany). Prior to the scan, recording electrodes were replaced with MRI-visible markers so the electrode positions could be obtained in the same coordinate system as the heart geometry. A navigated anatomical sequence was used so the ECGI electrical and anatomical data could be merged. Conventional cine imaging and advanced LGE imaging were conducted following the thorax scan. The contrast agent was 0.1mmol/Kg of Gadoterate meglumine (Dotarem, Guerbet S.A., Paris, France) with LGE images acquired 5-15 minutes post-contrast. The LGE sequence was a single shot steady state free precession phase sensitive inversion recovery sequence [14] with motion corrected averaging and high resolution (typical matrix: 144 x 256; voxel size 2.0 x 1.5 x 6.0 mm^3). Two patients declined contrast injection.

Unipolar epicardial electrograms (EGMs) were reconstructed using previously described methods [13] (additional ECGI methodology references in **Supplement**). Briefly, the heart-torso geometry obtained from the MRI was used to compute a transfer matrix relating epicardial

potentials to torso potentials. The inverse problem was solved to compute epicardial EGMs from the recorded ECGs. Typically, 1000 EGMs were computed over the entire ventricular epicardium. EGMs over the valve plane were excluded from analysis. Epicardial activation and repolarization maps were constructed from the EGMs. ECGI reconstructions of sinus rhythm were computed for each patient at resting HR prior to exercise and at elevated HR immediately after exercise cessation. Additionally, the epicardial activation sequence was computed for each unique premature ventricular contraction (PVC) morphology observed.

2.3.3 Analysis

Segmentation

ECGI maps and LGE images for each patient's ventricles were divided into basal, mid, and apical regions. Basal and mid regions were further subdivided into anterior, anterolateral, inferolateral, and inferior regions. Apical regions were subdivided into anterior and inferior regions. EGM measures for each region were computed as the mean value from all EGMs within the region.

CMR Analysis

CMR analysis was performed using CVI42 software (Circle Cardiovascular Imaging Inc.,Version 5.1.2[303], Calgary, Canada). For the analysis of LGE in the LV, epicardial and endocardial borders were manually drawn on the short axis slices and the anterior RV insertion point was identified. The Otsu semi-automated technique was used to quantify LGE and was displayed on a bullseye plot as relative enhanced area (percentage) per segment on the 16-segment American Heart Association model.

For the analysis of the RV LGE, a segmentation model was created using short axis images. Basal, mid and apical segments were identified using the papillary muscles as markers and divided into anterior, anterolateral, inferolateral and inferior segments for the basal and mid RV segments and as apical anterior and apical inferior segments for the RV apical segments.

The amount of RV LGE was quantified visually as 0 (no LGE), 1 (some LGE), or 2 (high LGE) independently by 2 operators with 3 years of experience in CMR each (SR and HB). The operators' RV LGE quantification differed initially in 2 segments. Following additional analysis of these segments, the reviewers reached a consensus. Analyses of the ECGI and CMR data were conducted independently with investigators blinded to the results of the other modality.

Electrogram Analysis

Reconstructed unipolar epicardial EGMs were processed to compute local electrical measures. Activation times (ATs) were computed as the time of steepest negative time-derivative of voltage ($-dV/dt_{max}$) in the local QRS complex. Recovery times (RTs) were computed as the time of steepest positive time-derivative (dV/dt_{max}) during the T-wave [15]. Activation-recovery intervals (ARIs, a surrogate for local action potential duration) were computed as the difference between RT and AT. **Supplemental Figure S2.2** defines these measures. ECGI-reconstructed ARI values were validated against direct intraoperative epicardial mapping in humans (Zhang et al. Online Supplement [16]). Spatial gradient magnitudes of EGM measures were computed for each EGM as the absolute value of the change between neighboring EGMs divided by the distance between EGM locations, averaged across all neighbors. EGM amplitudes were computed as the peak-to-peak voltage during the QRS complex. Fractionation was quantified using the number of steep downward deflections between QRS onset and the start of the T-wave.

Additional details of the fractionation quantification and sample EGMs are provided in **Supplemental Figure S2.3**. The earliest 10% of ATs were considered the epicardial initiation site of a PVC. PVC occurrence rates per EGM at a given epicardial site were computed as the number of times the EGM met the above criterion divided by the total number of beats recorded during the study.

Statistical Analysis

Fractionation values within anatomical segments are presented as z-scores compared to a group of 20 healthy adults. Electrical measures in the ARVC study population were compared to healthy controls using Wilcoxon rank-sum tests. Exercise changes were assessed using Wilcoxon signed-rank tests. Cohort data are presented as medians and quartiles. Substrate and PVC rate comparisons were performed using Spearman correlation coefficients computed using Matlab software (The MathWorks, Inc., Natick, Massachusetts, USA).

2.4 Results

2.4.1 Electrical Substrate at Rest

Abnormal sinus rhythm activation and conduction were common in the ARVC patients. The normal epicardial activation pattern is well described [17] and a representative control is presented in **Figure 2.1**. Generally, the earliest epicardial activation appears as a breakthrough, most commonly in the anterior RV, and the basal lateral LV is usually the latest region to activate (**Fig 2.1A**). The normal sinus activation of healthy adult hearts does not have regions of discontinuous conduction or fractionated EGMs (**Fig 2.1A and 2.1B, left**). In contrast to the normal activation sequence, we observed abnormal and varied epicardial breakthrough locations, regions of discontinuous conduction, and fractionated electrograms in the ARVC study population.

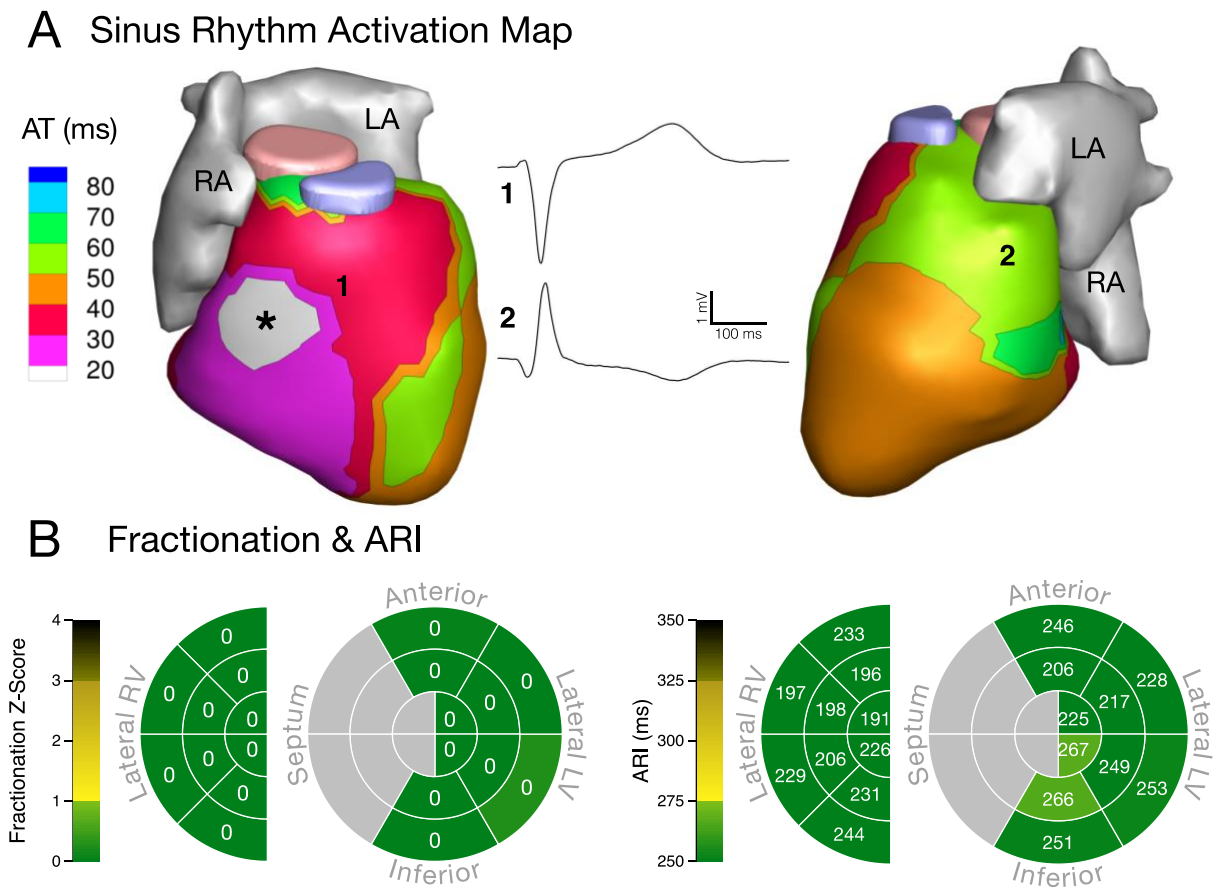

Figure 2.1 Electrical substrate in a healthy adult. (**A**) Sinus rhythm activation with a typical RV epicardial breakthrough (asterisk) and normal conduction. RV (1) and LV (2) unipolar EGMs have a normal morphology free of fractionation. (**B**) Schematic maps of normal electrical properties in anatomical regions based on 20 control subjects. Left: fractionation z-score. Right: Fridericia-corrected ARI. The maps show absence of fractionation and ARI values within the normal range. AT: activation time. RA: right atrium. LA: left atrium. RV: right ventricle. LV: left ventricle. ARI: activation-recovery interval. EGM: electrogram.

Figures 2.2-4 present activation and conduction patterns seen in ARVC patients. In two patients with advanced disease (63 and 66 years old, respectively) we observed earliest epicardial breakthrough in the LV (**Fig 2.2A** and **2.3A**). One of these patients had normal epicardial EGMs (**Fig 2.2A**), while we observed low-amplitude fractionated EGMs in the other (**Fig 2.3A**). ECGI resolved activation and conduction abnormalities in a 26-year-old patient who did not have any Major Task Force Diagnostic Criteria. In this patient, we observed fractionated EGMs and non-

uniform conduction near the earliest epicardial breakthrough site (**Fig 2.4A**). ARVC patients had fractionation scores within anatomical regions that ranged from values within the control range (**Fig 2.2B, top**) to values which were several standard deviations above the control distribution (**Fig 2.3B and 2.4B, top**). While some patients had high fractionation scores, we did not observe EGMs in these patients with deflections after the QRS complex (late potentials) that are commonly associated with re-entrant arrhythmias (**Fig 2.2A-4A**). The abnormal conduction in ARVC patients compared to controls was reflected in statistically longer total duration of epicardial activation ($p = 0.007$, Control: 42 [36-47] ms, ARVC: 52 [44-64] ms) and steeper mean epicardial gradients of AT ($p = 0.018$, Control: 0.24 [0.21-0.28] ms/mm, ARVC: 0.31 [0.26-0.37] ms/mm).

Repolarization in ARVC patients was prolonged compared to controls, and this prolongation was often spatially heterogeneous. **Figure 2.1B (right)** presents a schematic map of mean ARI values in epicardial segments for a representative control. Control values were homogenous and fell within the range of values previously reported [17]. In contrast, **Figures 2.2B and 2.3B (middle)** show prolonged ARI values in ARVC patients. As demonstrated in **Figure 2.2B (top)**, regions of normal ARI values may co-exist with regions of long ARIs. Mean ventricular ARIs during resting sinus rhythm (Fridericia rate correction applied) were significantly longer than control values ($p = 0.014$, Control: 241 [230-262] ms, ARVC: 275 [238-300] ms). While ARIs were prolonged in ARVC patients, we did not observe increased spatial gradients of repolarization or total duration of epicardial repolarization (**Supplemental Table S2.4**).

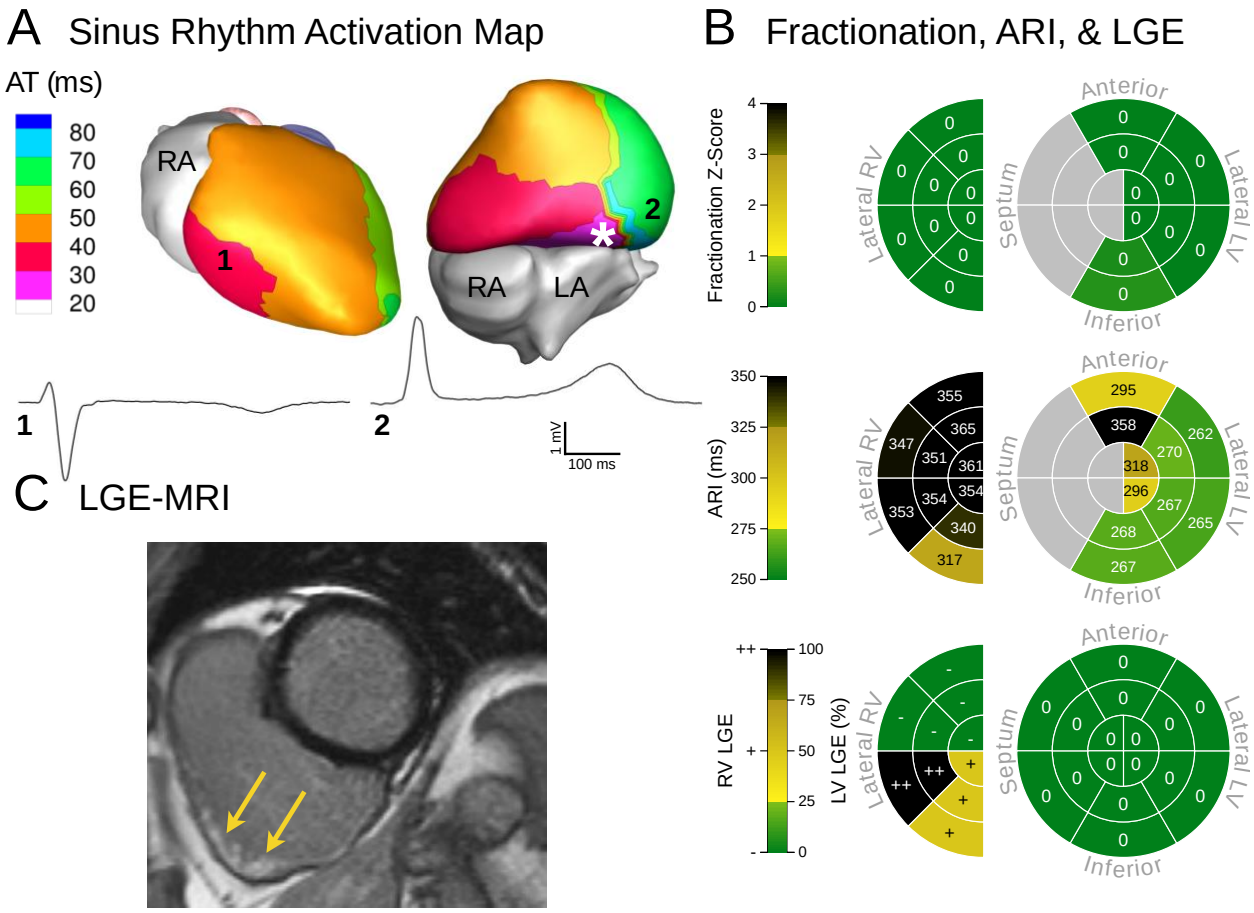

Figure 2.2 Electrical substrate of a patient (Patient 6) with advanced disease and a high PVC rate (18.69%). (**A**) Ventricular epicardial breakthrough during sinus rhythm was abnormal, with earliest activation originating from the basal inferior LV (asterisk). RV (1) and LV (2) unipolar EGMs had normal QRS morphology. (**B**) EGM fractionation was not abnormal compared to controls (top). Fridericia-corrected ARIs were prolonged compared to control values (middle). Concentrated LGE was visible in the inferior RV (bottom). (**C**) MRI image of extensive LGE, which was confined to the subepicardial RV (indicated by yellow arrows). PVC: premature ventricular contraction.

The presence of T-wave inversion on clinical ECG (clinical ECG findings in **Supplemental Table S2.2**) was strongly associated with ARI prolongation. ARVC patients with T-wave inversion (Fridericia rate correction applied) had significantly longer mean ARI values than those without inversion (p = 0.010, With Inversion: 300 [269-313] ms, Without Inversion: 238 [231-262] ms). However, ECGI identified a patient without T-wave inversion whose mean epicardial ARI was longer than any control, as well as a patient with T-wave inversion whose

mean epicardial ARI was within the lowest quartile of the control values (**Supplemental Table S2.5**).

As expected, mean epicardial ARI (uncorrected for HR) shortened due to exercise ($p < 0.001$). Total RT ($p = 0.002$), mean epicardial RT gradients ($p = 0.007$), and mean EGM amplitude ($p < 0.001$) also decreased due to exercise. Total AT, mean epicardial AT gradients, and fractionation were unaffected by exercise (**Supplemental Table S2.6**).

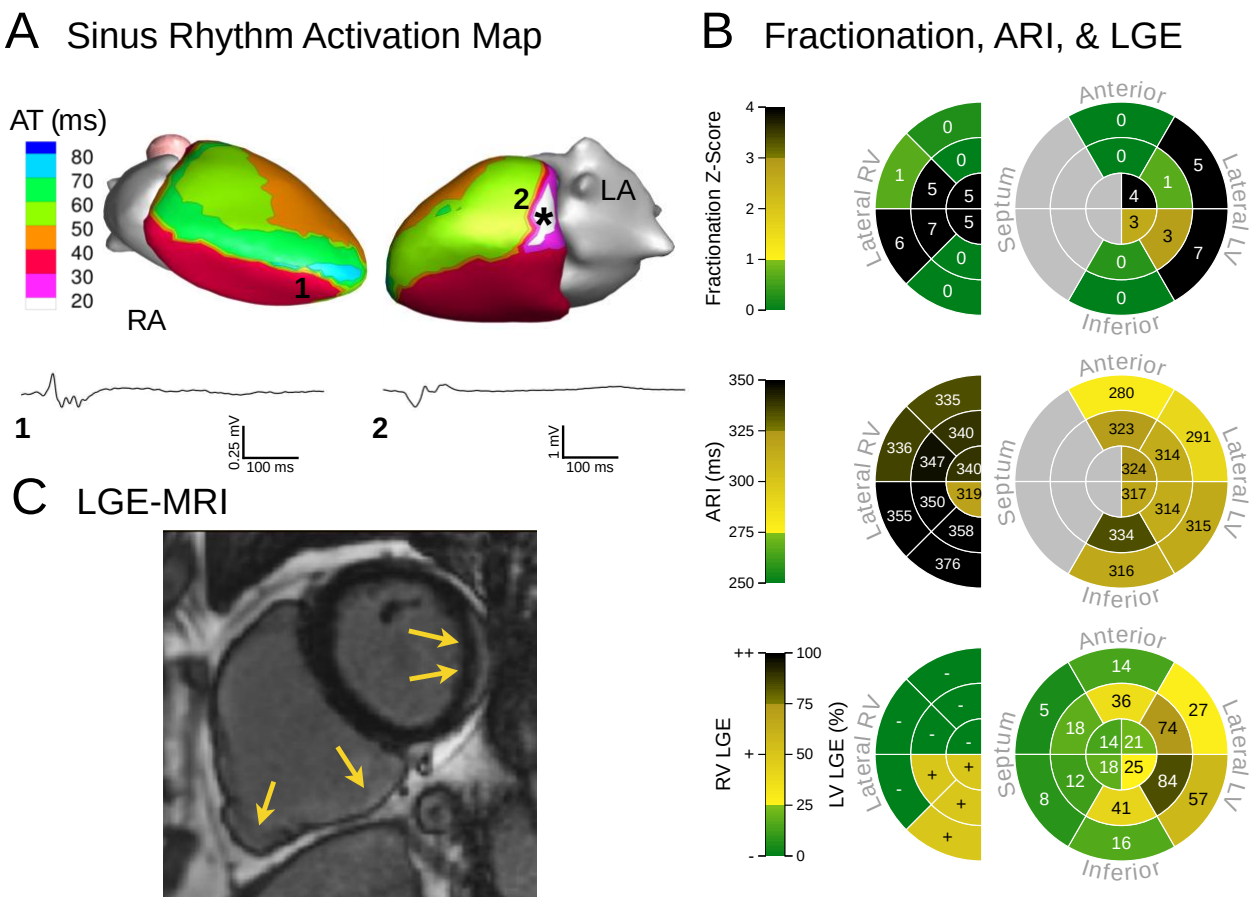

Figure 2.3 Electrical substrate of a patient (Patient 14) with biventricular disease and a moderate PVC rate (1.11%). (**A**) Sinus rhythm breakthrough was abnormal, with earliest epicardial activation originating from the basal lateral LV (asterisk). RV (1) and LV (2) unipolar EGMs were fractionated (note the voltage scale of low-amplitude EGM 1). (**B**) Regions of high fractionation were present in both ventricles (top), and Fridericia-corrected ARI values were prolonged compared to control values (middle). LGE was visible in both ventricles (bottom). (**C**) MRI image of LGE showing scar in both ventricles (yellow arrows).2.4.2 Electrical Substrate during Stress

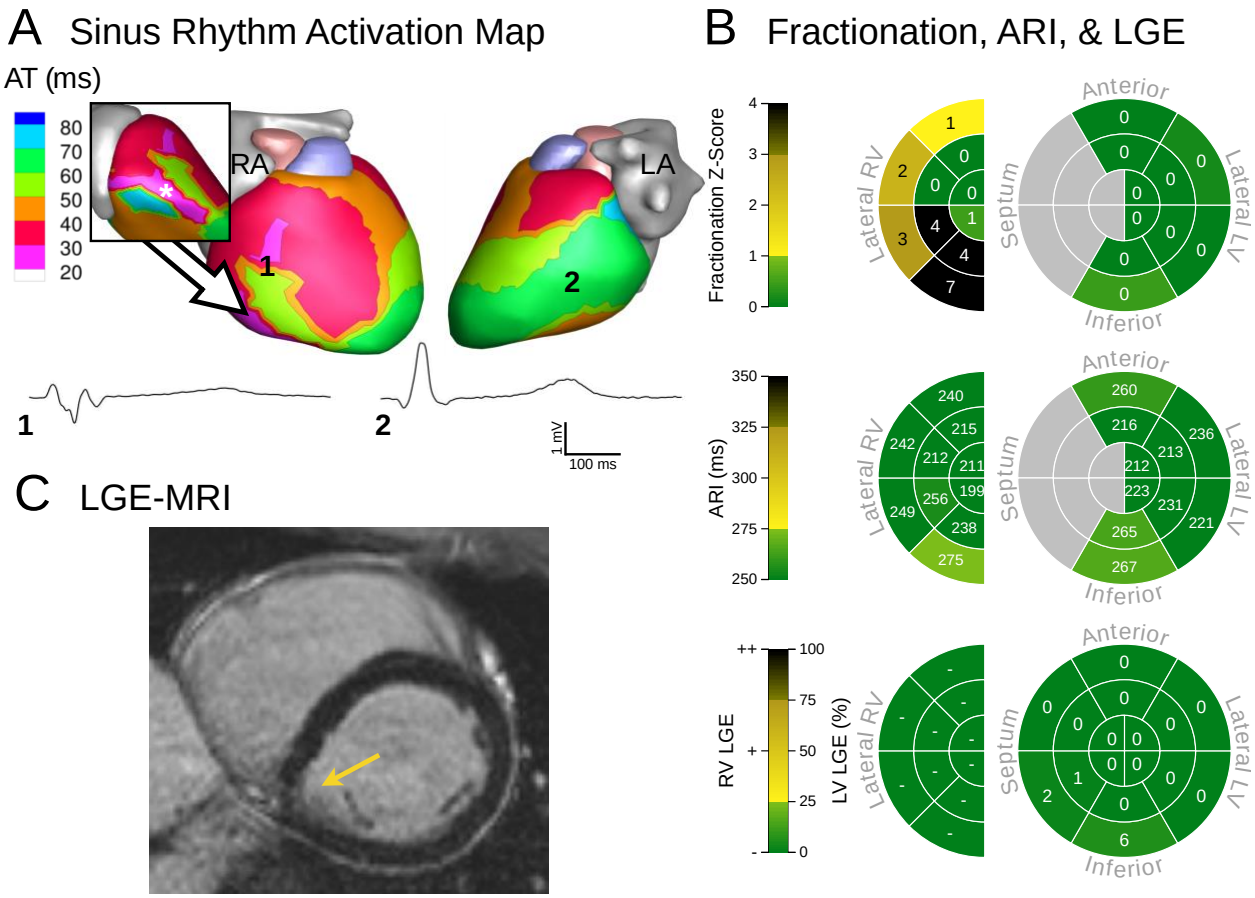

Figure 2.4 Electrical substrate of a 26-year-old male (Patient 13) with early disease and no observed PVCs. (**A**) Sinus rhythm epicardial breakthrough occurred in the inferolateral RV (asterisk in inset) with early activation of the RV free wall. There was a region of non-uniform conduction and fractionated unipolar EGMs (1) between these sites. Remote LV unipolar EGM (2) had a normal morphology. (**B**) Fractionation in the RV was much greater than control values (top) while Fridericia-corrected ARI values were within the normal range of controls (middle). Minimal LGE was visible in the LV (bottom). (**C**) MRI showed minimal abnormalities (arrow).

2.4.3 Structural (CMR) Substrate

Advanced LGE revealed a spectrum of scar burden in the ARVC patients. There was scar in 72% of ARVC patients agreeable to contrast. Three patients had isolated RV LGE, seven had isolated LV LGE, three had biventricular LGE, and five had no scar. Six patients in the study cohort had no Task Force CMR defects. Of these six, three had visible LV LGE. **Panels B (bottom) and C of Figures 2.2-4** illustrate the broad spectrum of LGE observed in the study population.

2.4.4 Relationship of Electrical and Structural Substrates

LGE scar spatially co-localized with EP substrate abnormalities, and the relationship between CMR scar and EP abnormalities was stronger in the LV than in the RV. The amount of LV LGE within anatomical segments correlated with EGM markers of abnormal depolarization including low amplitude EGMs, increased number of deflections per EGM, and increased AT spatial gradients. LV LGE correlated with prolonged resting ARI values and increase in ARI shortening during and post exercise (**Supplemental Table S2.7**). RV LGE values within anatomical segments did not correlate with EGM markers of abnormal depolarization, but did correlate with prolonged ARIs at rest and post-exercise. RV LGE correlated with ARI shortening due to exercise (**Supplemental Table S2.8**).

The results from Patient 6 (**Fig 2.2**) and Patient 14 (**Fig 2.3**) illustrate the above findings. Patient 6 has an RV anatomical scar that does not extend to the epicardium, as determined from LGE (**Fig 2.2C**). The absence of scar on the epicardium is reflected in the local EGMs (**EGM 1, Fig 2.2A**), which appear normal. This is also reflected in the normal fractionation z-scores (**Fig 2.2B, top**). Patient 14 has a similar RV anatomical scar, which lacks clear epicardial involvement (**Fig 2.3C**). However, in this case, the ECGI reconstructed epicardial EGMs at this location (**EGM 1, Fig 2.3A**) are low amplitude and fractionated, indicating EP abnormality at the epicardium. The same patient also has an LV scar which is visible on the epicardial aspect of the lateral LV. For this scar, the corresponding epicardial EGMs (**EGM 2, Fig 2.3A**) are fractionated, indicating coexistence of abnormal anatomical and EP substrates on the epicardium.

2.4.5 Ventricular Ectopy

Ventricular ectopy was common in the ARVC patients and occurred more frequently as heart rate increased following exercise. We observed PVCs in fifteen of twenty ARVC patients, with a total of 41 distinct morphologies. The sites of earliest epicardial activation of the PVCs were spread across both ventricles, with greater involvement of RV and basal locations. A schematic diagram of the earliest epicardial activation sites for all PVC morphologies is provided in **Figure 2.5**.

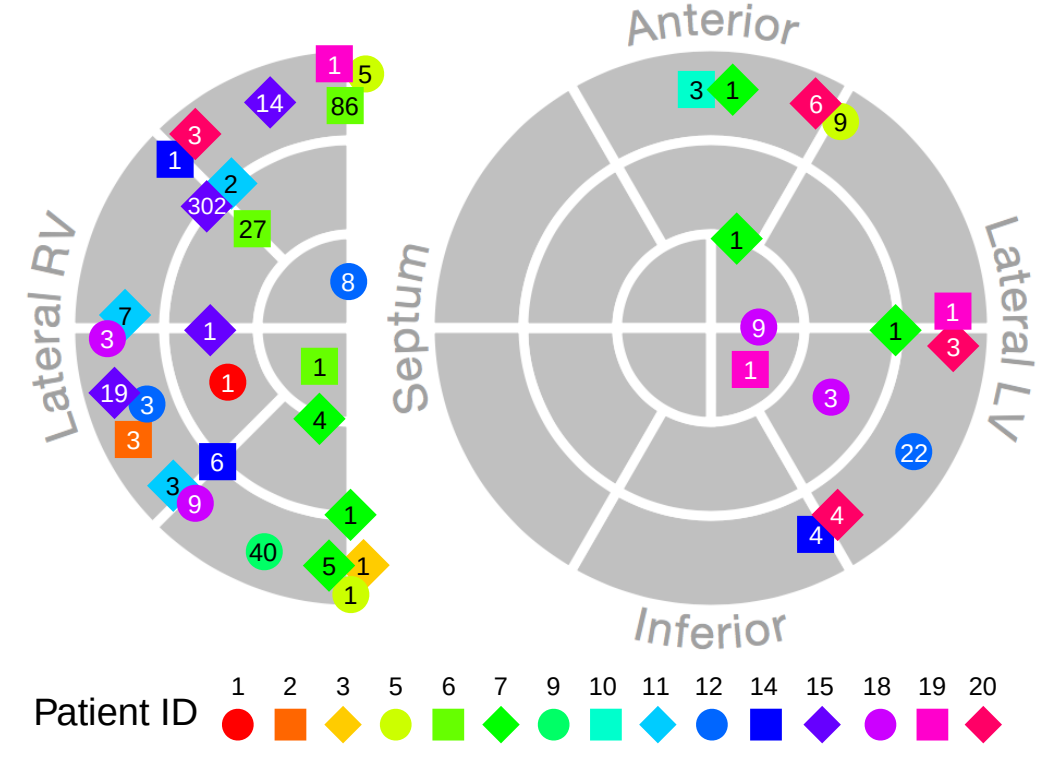

Figure 2.5 Schematic diagram of earliest epicardial activation of all observed PVC morphologies. Each marker represents a unique PVC morphology, with the number indicating the number of times the morphology was observed during the study. Marker color and shape identify patient ID (indicated below diagram). Sites near the epicardial aspect of the septum are shown on the edge of the RV.

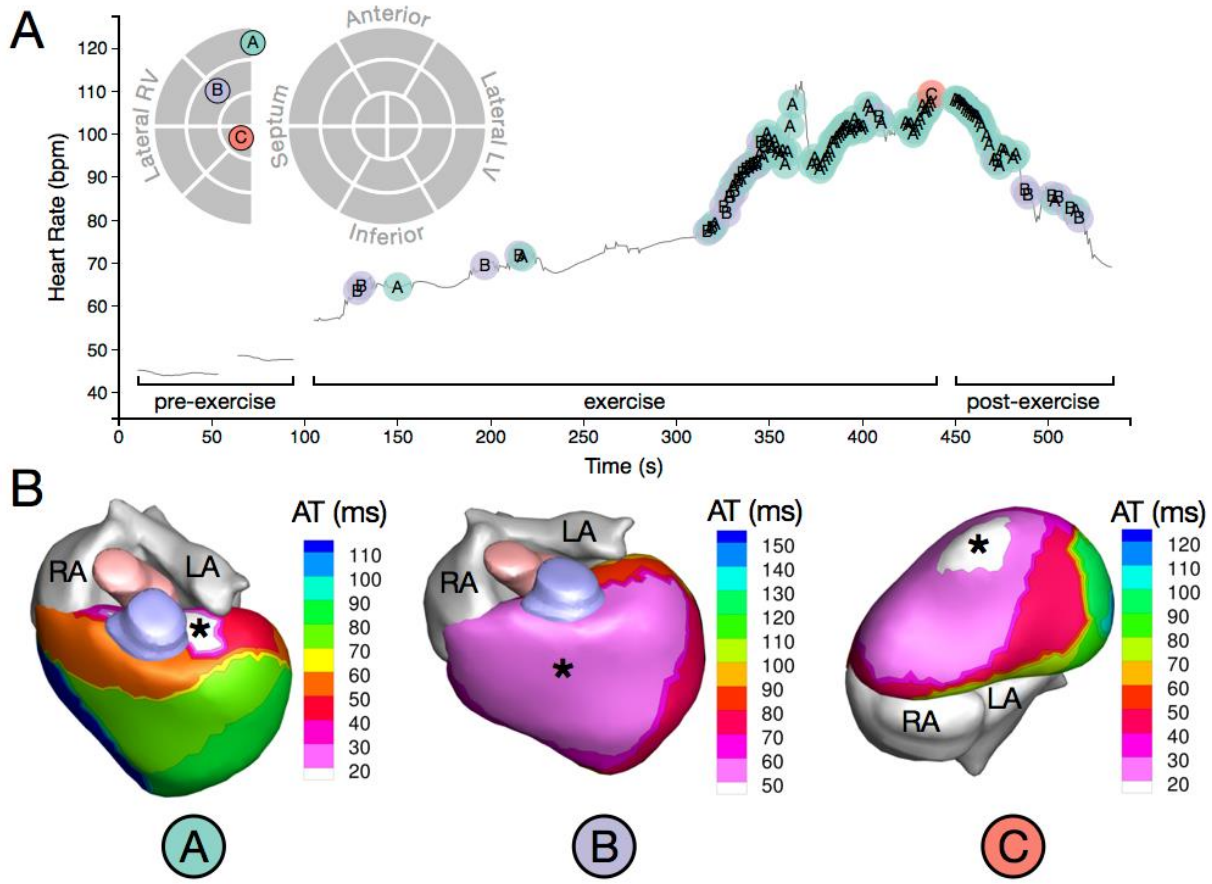

Figure 2.6 PVC onset and initiation sites of a patient (Patient 6) with a high PVC burden (18.69%). (A) Time-course of observed PVCs in relation to exercise and schematic map of PVC initiation sites. The different PVC initiation sites are labeled A, B, and C and color coded. PVCs occurred only after the onset of exercise, and morphology C appeared only once near peak HR (B) Activation isochrone maps of the three distinct PVC morphologies observed in this patient. Asterisks indicate PVC initiation sites. Morphology B showed very a broad region of early epicardial activation, indicating a possible sub-epicardial origin and possible conduction system involvement. HR: heart rate.

The PVC rate within anatomical segments correlated with prolonged ARIs, ARI shortening due to exercise, low voltage EGMs, increased deflections per EGM, and LGE scar (all correlations $p < 0.001$). The PVC rate within anatomical segments did not correlate with increased gradients in AT, RT, or ARI. **Figures 2.6** and **2.7** show the temporal occurrence and spatial location and propagation of PVCs in two patients. The substrates for these patients are presented in **Figures 2.2** and **2.3**, respectively. **Supplemental Table S2.9** summarizes the correlations between PVC rate and structural and EP substrate measures.

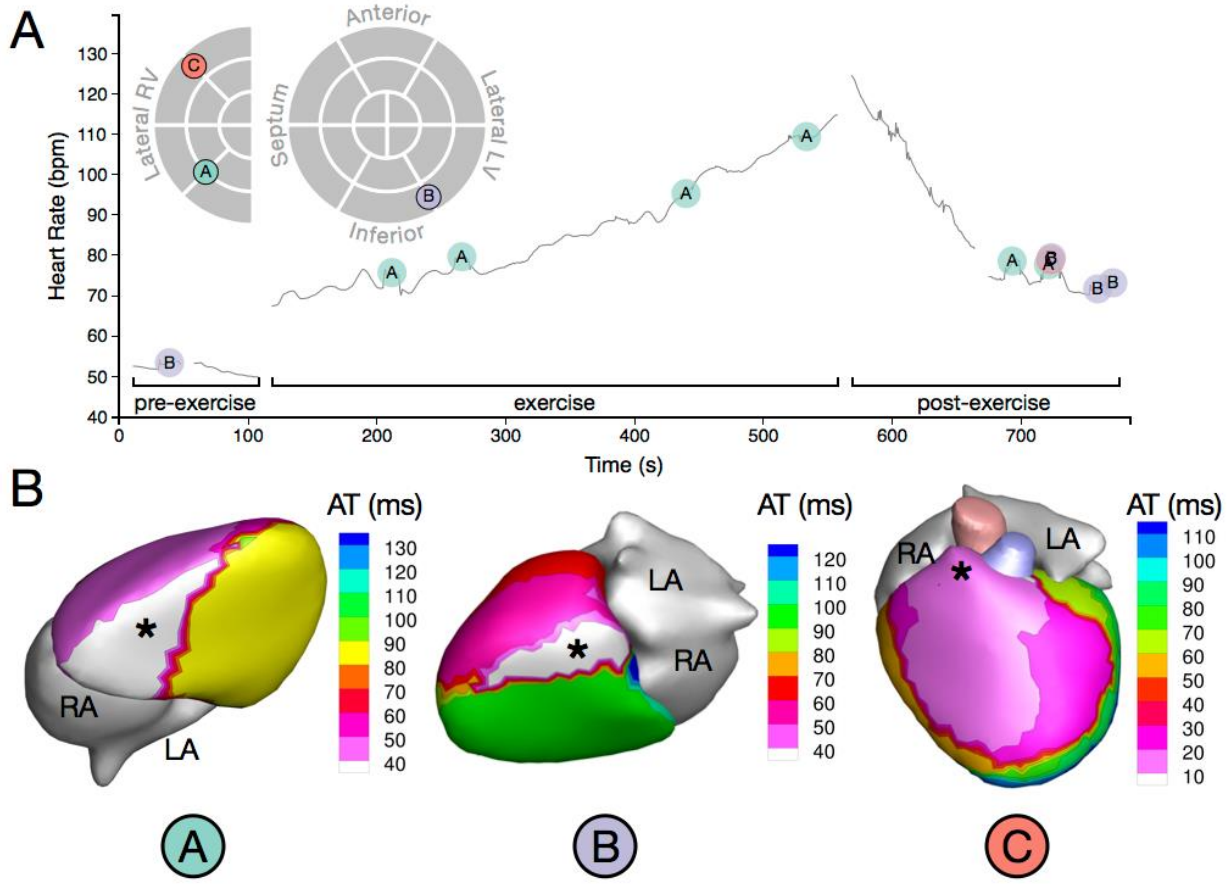

Figure 2.7 PVC onset and initiation sites of a patient (Patient 14) with a moderate PVC burden (1.11%). (A) Time-course of observed PVCs in relation to exercise and schematic map of PVC initiation sites. Note that morphology C is partially obscured in the post-exercise recording period. (B) Activation isochrone maps of the three distinct PVC morphologies observed in this patient. Asterisks indicate PVC initiation sites.

2.5 Discussion

This is the first evaluation of ECGI in ARVC patients. ECGI was sensitive enough to detect EP substrate differences between ARVC patients and healthy controls. By combining ECGI with LGE, we determined correlations between EP abnormalities and LGE scar. These correlations indicate that the EP abnormalities detected with ECGI are markers of disease progression. Importantly, new findings regarding properties of the EP and scar substrates included prolonged

epicardial ARIs and a relationship of PVC rate within a region to repolarization, EP markers of scar, and LGE.

2.5.1 ARVC Scar Substrate

Ventricular LGE was variable in location and extent. LV LGE was a more frequent finding than RV LGE. LV LGE co-localized with traditional markers of EP scar assessed using ECGI, as reflected by its correlation with lower voltage EGMs and increased fractionation. This finding mirrors prior ECGI studies that found regions of scar assessed with LGE or single-photon emission computed tomography to have lower voltage EGMs and increased fractionation [18]. In the RV, we did not observe a strong relationship between LGE and traditional EP markers of scar. This is consistent with prior work comparing invasive EP mapping to RV LGE, which found that nearly 50% of electrical scar substrates in the RV were not confirmed by LGE [19]. Prior studies have suggested that the absence of RV LGE findings could be attributed to the thin RV wall, which complicates LGE in the RV [20]. Alternatively, it is possible that EP abnormalities in the RV manifest in the presence of minimal scar or scar that is diffuse and not easily resolved with current imaging techniques.

2.5.2 Prolongation of Repolarization

There are multiple mechanisms which could contribute to the ARI prolongation observed in this study. Functional changes in ionic currents due to ARVC mutations could contribute to prolonged repolarization. Studies linking I_{Na} current to Plakophilin-2 mutations provided the first evidence that ARVC may have some features of a channelopathy [21]. While the focus of research efforts in this area has largely been on depolarization, it is possible that repolarizing currents are altered as well. $K_v1.5$ channels localize to the intercalated disc and associate with $Na_v1.5$ [22,23],

and $K_v1.5$ function depends on N-cadherin, an intercalated disc protein [24]. A mutation in KCNE2 that inhibits trafficking of $K_v1.5$ to the intercalated disc causes prolonged repolarization [25]. While we are unaware of direct evidence suggesting that this mechanism is involved in ARVC, it is an interesting avenue for exploration.

Another mechanism which may contribute to prolonged repolarization is progression of the heart failure phenotype associated with ARVC. Heart failure is a known end-stage complication of ARVC [4], but systolic impairment of varying degrees can appear in either or both ventricles in the absence of clinical heart failure [10]. Action potential prolongation is a hallmark of heart failure along with functional downregulation of potassium currents, slow conduction, and abnormal calcium homeostasis [26]. It is possible that these features develop in ARVC patients either globally or locally as the disease progresses and surviving myocardium is subjected to increasing strains because of fibrofatty tissue replacement.

Finally, myocardial uncoupling can increase the effects of any action potential duration prolongation mechanisms. Myocardial uncoupling facilitates gradients in repolarization by decreasing the electrotonic coupling between cells [27]. Fibrofatty replacement acts to uncouple cells by decreasing the local density of excitable cells. Reduction in the number and size of gap junctions in the intercalated disc causes further uncoupling in ARVC, and has been reported even in histologically normal regions of myocardium [6].

In our data, ARI prolongation correlated with LGE in both ventricles. This suggests that the uncoupling effect of the scar, altered mechanical strains in regions of scar, or both may be important to the development of prolonged repolarization. The uncoupling effect of ventricular scar could also contribute to the correlation we observed between stress-related ARI shortening

and LGE in both ventricles, as both rate increase and sympathetic stimulation have a greater effect on cardiomyocytes that are less electrically coupled. While our population size is not sufficient to draw conclusions about the age progression of the ARVC phenotype, we note that the group included two patients in their twenties, both of whom had ARI values within the normal range. This suggests that action potential prolongation in ARVC patients may develop as the overall phenotype progresses. Mean epicardial ARIs were generally longer in patients with precordial lead T-wave inversion. However, there were patients with and without T-wave inversion who were exceptions to this relationship, indicating that ECGI offers improved sensitivity and specificity for detecting prolonged repolarization. Additionally, ECGI provides spatial information about ARI prolongation, which was spatially heterogeneous in ARVC.

2.5.3 Arrhythmia Triggers (PVCs)

The ability of ECGI to panoramically map the whole heart in a single beat allowed us to localize PVCs, determine the frequency of each unique PVC morphology, and correlate ectopic frequency with the EP and scar substrates. The overall rate of PVCs was increased by exercise. We found that PVC rate within anatomical segments correlated with local ARI prolongation, increased ARI shortening due to exercise, low voltage EGMs, fractionated EGMs, and LGE.

The hallmark finding of progressive scar formation in ARVC is compatible with the possibility of re-entrant circuit formation. Prior work demonstrated conduction slowing at elevated heart rates in ARVC patients [28]. In the present study, we found evidence of slow conduction in the form of longer total activation times and steeper activation gradients relative to controls. However, we did not observe the dynamic conduction slowing at elevated HRs that Finlay et al. reported [28]. This discrepancy could be attributable to the difference in HRs investigated. In the

present study, patients exercised to a peak HR of 120 beats/min, whereas the patients in the Finlay et al. study were paced at an interval just below the ventricular refractory period.

The combination of scar, slow conduction, and prolonged repolarization could facilitate unidirectional block and reentrant arrhythmia. Important signatures of re-entrant arrhythmia are EGM fractionation and late potentials. We did not observe late potentials in the reconstructed EGMs. This stands in contrast to ECGI studies of post-infarction scar-related ventricular tachycardia, which found a high prevalence of late potentials with re-entry circuits closely related to the EP substrate [29]. While this could indicate that re-entrant arrhythmias are less prevalent in ARVC, it is important to note the significant differences in the anatomy of the scars in each population. Post–infarction scars are often large and heterogeneous, with large islands of surviving myocardium, especially in the border zone. The ARVC scar substrate, on the other hand, accumulates gradually over time and is typically diffuse, originating from the epicardium. It is possible that the lower regional density of surviving myocardium in ARVC scar makes it difficult to resolve late potentials in EP mapping of ARVC patients.

Focal mechanisms may cause arrhythmia triggers in ARVC patients. Focal triggered activity is commonly observed in isolated myocytes in the form of early afterdepolarizations or delayed afterdepolarizations. Early afterdepolarizatons at plateau potentials are caused by recovery and re-activation of I_{Ca}, with the delayed rectifier currents, I_{Kr} and I_{Ks}, playing an important role [30]. We observed that PVC rate correlated with regions of prolonged ARI, a surrogate for local action potential duration, including during stress when I_{Ca} is augmented by beta-adrenergic stimulation. Action potential duration prolongation increases the window for I_{Ca} re-activation and early afterdepolarization formation. In the intact heart, electrotonic coupling between myocytes acts as

a current sink for depolarizing currents. Reduced coupling, caused by scar and gap junction abnormalities in ARVC, can increase the likelihood of focal activity by decreasing the current sink effect. The observed correlation between PVC rate and electrical and LGE markers of scar suggests that an uncoupling effect is present at PVC initiation sites. It is interesting to note that Myles et al. [31] found that focal activity was more common in the RV, which they attributed to reduced coupling in the thin RV wall compared to the LV. In our study, we found greater overall ectopy in the RV.

2.5.4 Clinical Implications

The progressive nature of ARVC and its early concealed phase complicate diagnosis and treatment. CMR currently plays a valuable role in the evaluation of ventricular structure and function. The current Task Force criteria do not include LGE, but acknowledge that it may be included in future revisions [3]. Our data show that combined ECGI and LGE could increase the sensitivity for detecting substrate abnormalities in ARVC patients, including young patients with little or no Task Force MRI and ECG criteria. LGE and ECGI are compatible with the current use of CMR in the diagnosis and longitudinal assessment of ARVC. These imaging techniques can be performed in addition to the conventional CMR assessment to provide a thorough characterization of structural, functional, and EP abnormalities. In the present study, we report a spectrum of abnormalities using these techniques and demonstrate a relationship between the imaged substrates and ventricular ectopy. Since ventricular ectopy may play a causal role in triggering arrhythmias, combined ECGI and LGE may have a role in risk stratification.

2.5.5 Limitations

This study is a first evaluation of combined ECGI and LGE in ARVC patients and, therefore, evaluated a relatively small group of twenty patients. Because CMR is commonly contraindicated in patients with implanted devices, we only recruited patients without ICDs. While this choice enabled us to image LGE in the study cohort, a drawback is that none of the patients in this study had prior episodes of ventricular tachycardia. Therefore, this study cohort is not well-suited for evaluating sudden cardiac death risk stratification. Further studies are necessary to explore this application of these techniques. The current study evaluated patients ranging in age from 24 to 75 years old; however, only three patients were younger than 41 years old. Future studies should evaluate whether this approach can detect the presence of ARVC in young, asymptomatic and genotype-positive individuals. Larger studies of a wide range of ages and genotypes are important for exploring the progression of the disease, including how the EP and scar substrates change over time. Prior studies demonstrated that strain imaging may be effective for detecting the early stages of ARVC and for risk stratification [32,33]. Future studies could combine ECGI and strain imaging into a multi-modality approach for ARVC diagnosis and risk stratification. Exercise and LGE data were collected from the ARVC patients, but not controls. These data are needed to establish ranges for healthy controls. Additional data are necessary to determine the specificity of ECGI and LGE criteria for diagnosis of ARVC.

2.5.6 Conclusion

ECGI in combination with advanced LGE reveals a spectrum of electrical and structural substrate abnormalities in ARVC patients. This combination may improve sensitivity for detecting ARVC substrate abnormalities. These data suggest a role for combined ECGI and LGE in early diagnosis, non-invasive follow-up, and risk stratification of ARVC patients.

Chapter 2 References

1. Sen-Chowdhry S, Morgan RD, Chambers JC, McKenna WJ. Arrhythmogenic cardiomyopathy: etiology, diagnosis, and treatment. *Annu Rev Med*. 2010;61:233–253.

2. Asimaki A, Kleber AG, Saffitz JE. Pathogenesis of Arrhythmogenic Cardiomyopathy. *Can J Cardiol*. 2015;31:1313–1324.

3. Marcus FI, McKenna WJ, Sherrill D, Basso C, Bauce B, Bluemke DA, Calkins H, Corrado D, Cox MGPJ, Daubert JP, Fontaine G, Gear K, Hauer R, Nava A, Picard MH, Protonotarios N, Saffitz JE, Sanborn DMY, Steinberg JS, Tandri H, Thiene G, Towbin JA, Tsatsopoulou A, Wichter T, Zareba W. Diagnosis of Arrhythmogenic Right Ventricular Cardiomyopathy/Dysplasia: Proposed Modification of the Task Force Criteria. *Circulation*. 2010;121:1533–1541.

4. Corrado D, Wichter T, Link MS, Hauer RNW, Marchlinski FE, Anastasakis A, Bauce B, Basso C, Brunckhorst C, Tsatsopoulou A, Tandri H, Paul M, Schmied C, Pelliccia A, Duru F, Protonotarios N, Estes NM, McKenna WJ, Thiene G, Marcus FI, Calkins H. Treatment of Arrhythmogenic Right Ventricular Cardiomyopathy/Dysplasia: An International Task Force Consensus Statement. American Heart Association Journals; 2015. p. 441–453.

5. Basso C, Thiene G, Corrado D, Angelini A, Nava A, Valente M. Arrhythmogenic right ventricular cardiomyopathy. Dysplasia, dystrophy, or myocarditis? *Circulation*. 1996;94:983–991.

6. Delmar M, McKenna WJ. The cardiac desmosome and arrhythmogenic cardiomyopathies: from gene to disease. *Circ Res*. 2010;107:700–714.

7. Cerrone M, Delmar M. Desmosomes and the sodium channel complex: implications for arrhythmogenic cardiomyopathy and Brugada syndrome. *Trends Cardiovasc Med*. 2014;24:184–190.

8. Rojas A, Calkins H. Present understanding of the relationship between exercise and arrhythmogenic right ventricular dysplasia/cardiomyopathy. *Trends Cardiovasc Med*. 2015;25:181–188.

9. Gomes J, Finlay M, Ahmed AK, Ciaccio EJ, Asimaki A, Saffitz JE, Quarta G, Nobles M, Syrris P, Chaubey S, McKenna WJ, Tinker A, Lambiase PD. Electrophysiological abnormalities precede overt structural changes in arrhythmogenic right ventricular

cardiomyopathy due to mutations in desmoplakin-A combined murine and human study. *European heart journal*. 2012;33:1942–1953.

10. Sen-Chowdhry S, Syrris P, Ward D, Asimaki A, Sevdalis E, McKenna WJ. Clinical and genetic characterization of families with arrhythmogenic right ventricular dysplasia/cardiomyopathy provides novel insights into patterns of disease expression. *Circulation*. 2007;115:1710–1720.

11. Zorzi A, Rigato I, Bauce B, Pilichou K, Basso C, Thiene G, Iliceto S, Corrado D. Arrhythmogenic Right Ventricular Cardiomyopathy: Risk Stratification and Indications for Defibrillator Therapy. *Curr Cardiol Rep*. 2016;18:57–11.

12. Marchlinski FE, Edvardsen T. Arrhythmogenic Right Ventricular Cardiomyopathy: Better Tools for Detecting Early Disease and Progression. *J Am Coll Cardiol*. 2016;68:2198–2200.

13. Ramanathan C, Ghanem RN, Jia P, Ryu K, Rudy Y. Noninvasive electrocardiographic imaging for cardiac electrophysiology and arrhythmia. *Nat Med*. 2004;10:422–428.

14. Kellman P, Arai AE. Cardiac imaging techniques for physicians: late enhancement. *J Magn Reson Imaging*. 2012;36:529–542.

15. Coronel R, Debakker J, Wilmsschopman F, Opthof T, Linnenbank A, Belterman C, Janse M. Monophasic action potentials and activation recovery intervals as measures of ventricular action potential duration: Experimental evidence to resolve some controversies. *Heart Rhythm*. 2006;3:1043–1050.

16. Zhang J, Hocini M, Strom M, Cuculich PS, Cooper DH, Sacher F, Orini M, Lambiase PD, Taggart P, Haïssaguerre M, Rudy Y (With contribution to Section 1 of Online Supplement by Orini M, Lambiase PD, Taggart P). The Electrophysiological Substrate of Early Repolarization Syndrome: Noninvasive Mapping in Patients. *J Am Coll Cardiol EP*. In Press.

17. Ramanathan C, Jia P, Ghanem R, Ryu K, Rudy Y. Activation and repolarization of the normal human heart under complete physiological conditions. *Proc Natl Acad Sci USA*. 2006;103:6309–6314.

18. Cuculich PS, Zhang J, Wang Y, Desouza KA, Vijayakumar R, Woodard PK, Rudy Y. The electrophysiological cardiac ventricular substrate in patients after myocardial infarction: noninvasive characterization with electrocardiographic imaging. *J Am Coll Cardiol*. 2011;58:1893–1902.

19. Marra MP, Leoni L, Bauce B, Corbetti F, Zorzi A, Migliore F, Silvano M, Rigato I, Tona

F, Tarantini G, Cacciavillani L, Basso C, Buja G, Thiene G, Iliceto S, Corrado D. Imaging study of ventricular scar in arrhythmogenic right ventricular cardiomyopathy: comparison of 3D standard electroanatomical voltage mapping and contrast-enhanced cardiac magnetic resonance. *Circulation Arrhythmia and electrophysiology*. 2012;5:91–100.

20. Riele Te ASJM, Tandri H, Bluemke DA. Arrhythmogenic right ventricular cardiomyopathy (ARVC): cardiovascular magnetic resonance update. *J Cardiovasc Magn Reson*. 2014;16:50.

21. Sato PY, Musa H, Coombs W, Guerrero-Serna G, Patiño GA, Taffet SM, Isom LL, Delmar M. Loss of plakophilin-2 expression leads to decreased sodium current and slower conduction velocity in cultured cardiac myocytes. *Circ Res*. 2009;105:523–526.

22. Mays DJ, Foose JM, Philipson LH, Tamkun MM. Localization of the Kv1.5 K+ channel protein in explanted cardiac tissue. *J Clin Invest*. 1995;96:282–292.

23. Milstein ML, Musa H, Balbuena DP, Anumonwo JMB, Auerbach DS, Furspan PB, Hou L, Hu B, Schumacher SM, Vaidyanathan R, Martens JR, Jalife J. Dynamic reciprocity of sodium and potassium channel expression in a macromolecular complex controls cardiac excitability and arrhythmia. *Proc Natl Acad Sci USA*. 2012;109:E2134–43.

24. Cheng L, Yung A, Covarrubias M, Radice GL. Cortactin is required for N-cadherin regulation of Kv1.5 channel function. *J Biol Chem*. 2011;286:20478–20489.

25. Roepke TK, Kontogeorgis A, Ovanez C, Xu X, Young JB, Purtell K, Goldstein PA, Christini DJ, Peters NS, Akar FG, Gutstein DE, Lerner DJ, Abbott GW. Targeted deletion of kcne2 impairs ventricular repolarization via disruption of I(K,slow1) and I(to,f). *FASEB J*. 2008;22:3648–3660.

26. Aiba T, Tomaselli GF. Electrical remodeling in the failing heart. *Curr Opin Cardiol*. 2010;25:29–36.

27. Viswanathan PC, Shaw RM, Rudy Y. Effects of IKr and IKs heterogeneity on action potential duration and its rate dependence: a simulation study. *Circulation*. 1999;99:2466–2474.

28. Finlay MC, Ahmed AK, Sugrue A, Bhar-Amato J, Quarta G, Pantazis A, Ciaccio EJ, Syrris P, Sen-Chowdhry S, Ben-Simon R, Chow AW, Lowe MD, Segal OR, McKenna WJ, Lambiase PD. Dynamic conduction and repolarisation changes in early arrhythmogenic right ventricular cardiomyopathy versus benign outflow tract ectopy demonstrated by high density mapping & paced surface ECG analysis. *PLoS ONE*. 2014;9:e99125.

29. Zhang J, Cooper DH, Desouza KA, Cuculich PS, Woodard PK, Smith TW, Rudy Y. Electrophysiologic Scar Substrate in Relation to VT: Noninvasive High-Resolution Mapping and Risk Assessment with ECGI. *Pacing Clin Electrophysiol*. 2016;39:781–791.

30. Zeng J, Rudy Y. Early afterdepolarizations in cardiac myocytes: mechanism and rate dependence. *BPJ*. 1995;68:949–964.

31. Myles RC, Wang L, Kang C, Bers DM, Ripplinger CM. Local β-adrenergic stimulation overcomes source-sink mismatch to generate focal arrhythmia. *Circ Res*. 2012;110:1454–1464.

32. Mast TP, Teske AJ, Walmsley J, Van Der Heijden JF, van Es R, Prinzen FW, Delhaas T, van Veen TA, Loh P, Doevendans PA, Cramer MJ, Lumens J. Right Ventricular Imaging and Computer Simulation for Electromechanical Substrate Characterization in Arrhythmogenic Right Ventricular Cardiomyopathy. *J Am Coll Cardiol*. 2016;68:2185–2197.

33. Sarvari SI, Haugaa KH, Anfinsen OG, Leren TP, Smiseth OA, Kongsgaard E, Amlie JP, Edvardsen T. Right ventricular mechanical dispersion is related to malignant arrhythmias: a study of patients with arrhythmogenic right ventricular cardiomyopathy and subclinical right ventricular dysfunction. *European heart journal*. 2011;32:1089–1096.

Chapter 2 Appendix

Supplemental Figure S2.1: The ECGI Procedure

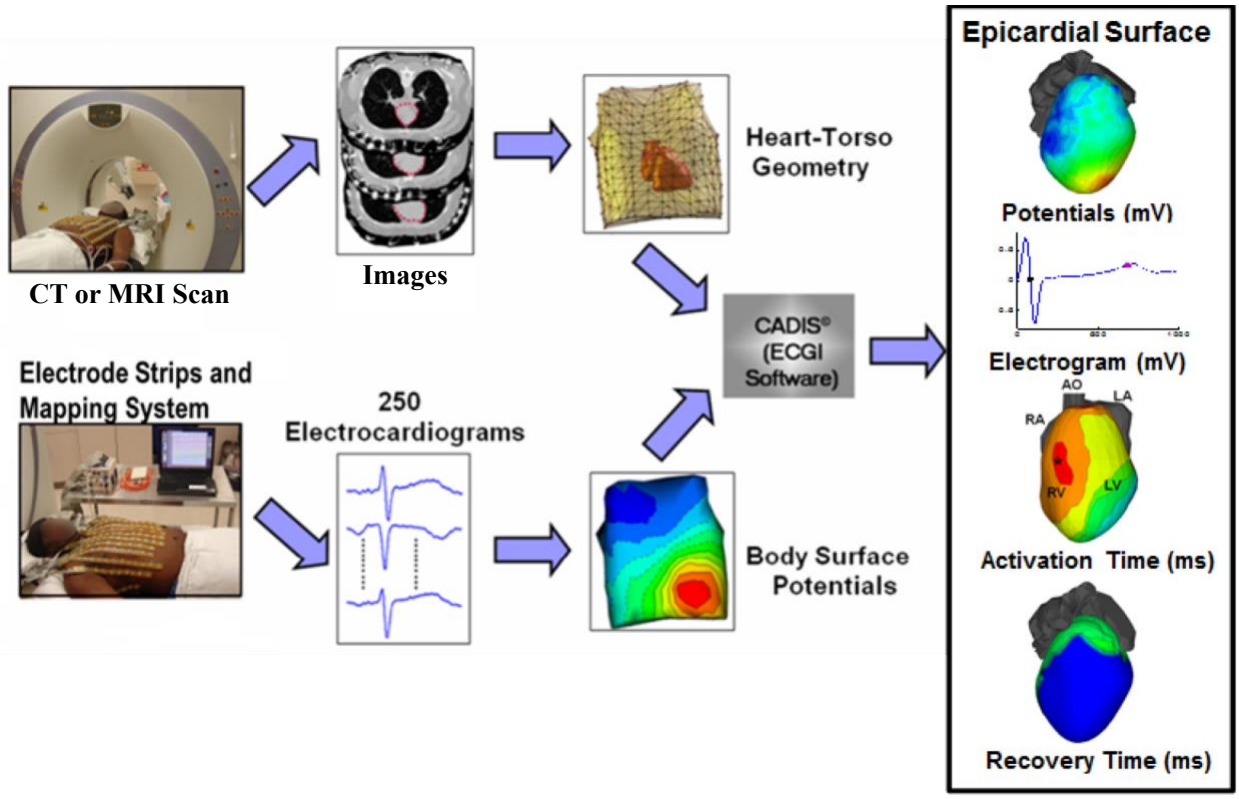

Schematic diagram of the ECGI procedure. A computed tomography (CT) or magnetic resonance imaging (MRI) scan provides the geometry of the epicardial surface and the locations of the recording electrodes on the body surface in the same coordinate system (top). The body surface potential distribution is obtained from 256 simultaneously recorded electrocardiograms (bottom). Solving the inverse problem (middle gray box) yields epicardial potentials and electrograms, from which activation times, recovery times, and other parameters of interest are derived (right frame).

Supplemental Figure S2.2: Activation Time, Recovery Time, and Activation-Recovery Intervals

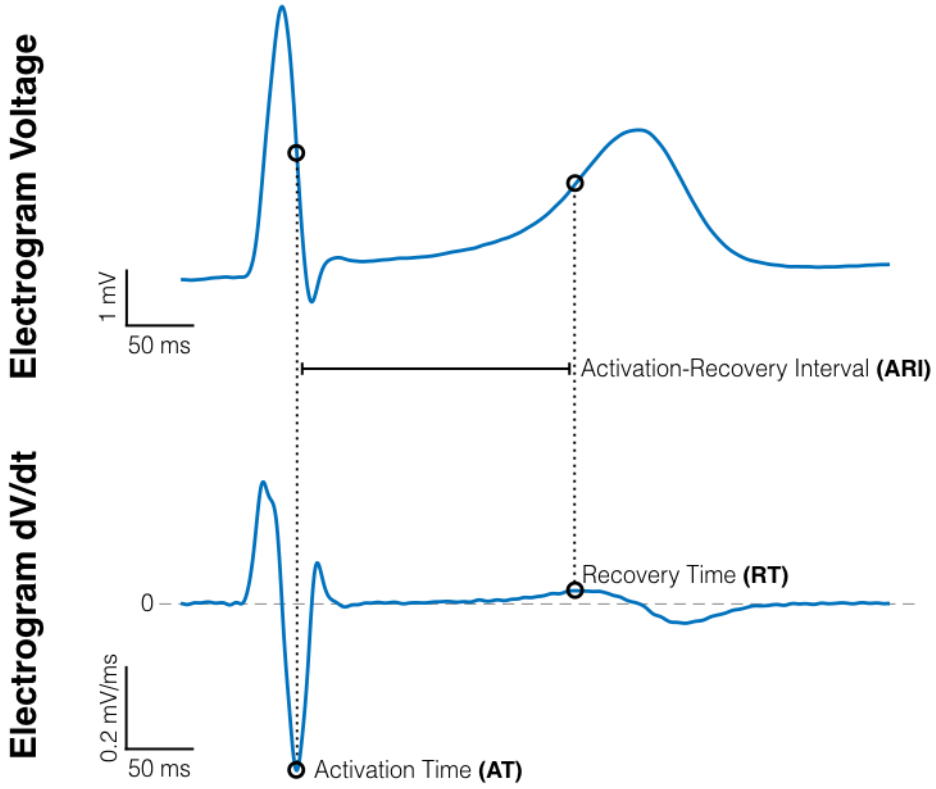

Diagram of unipolar electrogram (EGM) Activation Time (AT), Recovery Time (RT), and Activation-Recovery Interval (ARI). Temporal derivatives (bottom) were computed from EGMs (top). ATs were computed as the time of steepest negative time-derivative of voltage ($-dV/dt_{max}$) in the local QRS complex. Recovery Times were computed as the time of steepest positive time-derivative (dV/dt_{max}) during the T-wave. To eliminate noise effects from RT values, T-waves were lowpass-filtered using a 30 Hz Butterworth filter before determining RT. ARIs (a surrogate for local action potential duration) were computed as the difference between RT and AT.

EGM: electrogram
AT: Activation Time
RT: Recovery Time
ARI: Activation-Recovery Interval

Supplemental Figure S2.3: Electrogram Fractionation

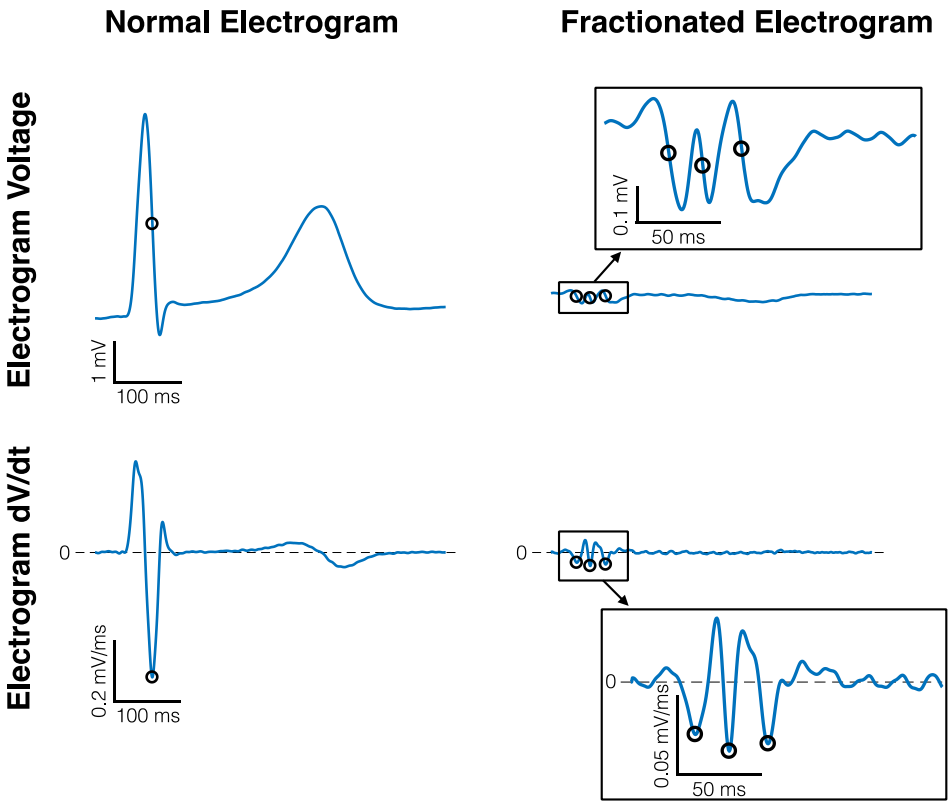

Diagram of electrogram (EGM) deflections for a normal EGM (left) and a low-amplitude fractionated EGM (right, shown on the same scale). The normal EGM had a single deflection (left, circle) while the fractionated EGM had 3 deflections (right, circles). Insets (large box) show fractionated EGM QRS voltage and dV/dt on enlarged scale. Fractionation was quantified by counting the number of steep downward deflections between the QRS onset and the start of the T-wave. Temporal derivatives (dV/dt, bottom) were computed from unipolar EGMs (top). Downward deflections were regions of EGMs with a negative dV/dt. Multiple deflections occurred when there was a positive dV/dt between downward deflections. The thresholds for steep downward deflections were:

1) Deflection peak-to-peak voltage amplitude ≥ 10% of the EGM peak-to-peak voltage amplitude
2) Deflection –dV/dt ≥ 70% of the EGM maximum –dV/dt
Additionally, both values were required to be ≥ 5% of the corresponding median values for all EGMs to prevent the detection of noise in flat EGMs as fractionation.

EGM: electrogram

Supplemental Table S2.1: Manuscript Abbreviations

Abbreviation	Meaning
ARVC	Arrhythmogenic Right Ventricular Cardiomyopathy
RV	Right Ventricle
LV	Left Ventricle
EP	Electrophysiological
ICD	Implantable Cardioverter Defibrillator
ECGI	Electrocardiographic Imaging
MRI	Magnetic Resonance Imaging
CMR	Cardiac Magnetic Resonance
LGE	Late Gadolinium Enhancement
ECG	Electrocardiogram
HR	Heart Rate
EGM	Electrogram
PVC	Premature Ventricular Contraction
AT	Activation Time
RT	Recovery Time
ARI	Activation-Recovery Interval

Supplemental Table S2.2: Patient Clinical Characteristics

Demographics			Genetics		RV Morphological Abnormalities					LV Morphological Abnormalities					Scar			ECG Abnormalities				Arrhythmias					Task Force Criteria	
ID	Age	Gender	Gene	Mutation	Dilation	Wall Thinning	RWMA	Systolic Dysfunction	Anurysm	Dilation	Wall Thinning	RWMA	Systolic Dysfunction	Anurysm	RV LGE	LV LGE	Biopsy	T wave Inversion	Epsilon Waves	Positive SAECG	Terminal 5 wave >55ms	NSVT/SVT superior axis	NSVT/SVT indeterminate or inferior axis	>500 VE's per 24hrs	VT Inducible	Study History	Family History	Major	Minor
1	59	M	JUP	JUP:c.2039G>A,p.W680X	+	-	-	-	-	-	-	-	-	-	-	+		-	-	-	-	-	-	-			Major	1	1
2	63	M	PKP2	c.148_151delACAG,p.S50fsX110*	+	-	+	-	-	-	-	-	-	-	-	-		-	-	+	-	-	-	+			Major	1	3
3	54	F	PKP2	c.1799delA,p.V600fsX655	+	-	+	-	-	-	-	+	-	-	-	-		V1-3	-	-	-	-	+	+			Major	2	3
4	44	M	DSP	c.817_818insA,p.Q273fsX288	-	-	-	-	-	-	-	-	-	-	-	-		-	-	+	+	-	+	-	-		Major	1	3
5	55	M	DSP	c.G4477T:p.E1493X	+	-	-	-	-	-	-	-	-	-	-	+		-	-	+	-	-	+	+			Major	1	5
6	63	M	PKP2	c.2197_2202delinsG,p.A733fsX740	+	+	+	+	-	-	+	+	-	-	+	-	+	V1-4	-	-	+	-	-	+			Minor	3	3
7	59	M	DSP	c.3045delG,p.S1015fsX1017	+	-	-	-	-	-	-	+	+	-	-	+		V1-5	-	-	-	-	+	+			Minor	1	3
8	69	F	PKP2	c.2146-1G>C	-	-	-	-	-	-	-	-	-	-	-	-		-	-	-	-	-	+	+			Minor	0	2
9	61	M	DSP	c.G4477T:p.E1493X	-	-	-	-	-	-	-	-	-	-	-	+		V5-6	-	-	-	-	+	+			Major	1	2
10	41	F	DSP	c.C5178A:p.N1726K*	-	-	-	-	-	-	-	-	-	-	-	-		V1-4	-	-	-	-	-	-			Minor	1	1
11	49	F	PKP2	c.2489+1G>A	+	-	+	-	-	-	-	-	-	-	+	-		V1-4	-	+	-	-	-	+			Major	3	2
12	60	M	DSG	c.G3C:p.M1I	+	-	+	-	-	-	-	+	+	+				V5-6	-	+	-	-	-	+			Major	3	2
13	26	M	PKP2	c.2489+1G>A	-	-	-	-	-	-	-	-	-	-	-	+		-	-	+	+	-	-	-			Minor	0	3
14	66	M	PKP2	c.2197_2202delinsG,p.A733fsX740	+	-	+	+	-	-	+	+	-	-	+	+		V1-3	-	-	+	-	-	-			Major	2	1
15	54	M	PKP2	c.2146-1G>C	-	-	+	-	+	-	-	-	-	-	+	-		V1-4	-	-	-	-	-	-			Major	2	0
16	74	M	DSG	c.G3C:p.M1I	-	-	+	-	-	-	-	-	-	-				-	+	+	-	-	-	+			Minor	1	3
17	24	M	DSP	c.C3337T:p.R1113X	-	-	-	-	-	-	-	-	-	-	-	+		-	-	-	-	-	-	-			Major	1	0
18	54	M	-	Desmosomal gene negative	-	-	+	-	+	-	+	+	-	-	+	+	+	V1-6	-	-	-	-	-	+			None	2	2
19	39	M	-	Desmosomal gene negative	+	-	+	-	-	+	-	+	-	-	-	+		V1-4	-	-	-	-	+	+			None	2	2
20	75	M	-	Desmosomal gene negative	-	-	+	+	-	-	+	+	-	-	+	+	+	V1-5	-	-	-	+	-	+			None	2	3

Clinical characteristics of ARVC study population. Asterisk indicates gene variant of unknown significance.

JUP: Plakoglobin
PKP2: Plakophilin-2
DSP: Desmoplakin
DSG: Desmoglein
RWMA: Regional Wall Motion Abnormality
LV: Left Ventricular
RV: Right Ventricular
LGE: Late Gadolinium Enhancement
SAECG: Signal Averaged Electrocardiogram
NSVT: Non-Sustained Ventricular Tachycardia
SVT: Sustained Ventricular Tachycardia
VE: Ventricular Extrasystole
VT: Ventricular Tachycardia

Supplemental Table S2.3: Holter PVC Findings

ID	Age	Gender	PVC Count	Monomorphic/Poloymorphic	Morphology
1	59	M	59	Monomorphic	LBBB
2	63	M	620	Polymorphic	LBBB+RBBB
3	54	F	1028	Monomorphic	LBBB
4	44	M	10	Monomorphic	LBBB
5	55	M	1000	Monomorphic	LBBB
6	63	M	2364	Monomorphic	LBBB
7	59	M	1111	Polymorphic	LBBB+RBBB
8	69	F	784	Monomorphic	LBBB
9	61	M	>3000	Monomorphic	LBBB
10	41	F	56	Monomorphic	LBBB
11	49	F	642	Monomorphic	LBBB
12	60	M	681	Polymorphic	LBBB+RBBB
13	26	M	52	Monomorphic	LBBB
14	66	M	26	Monomorphic	LBBB
15	54	M	38	Monomorphic	LBBB
16	74	M	1056	Monomorphic	LBBB
17	24	M	56	Monomorphic	LBBB
18	54	M	3496	Monomorphic	LBBB
19	39	M	890	Monomorphic	LBBB
20	75	M	>3000	Monomorphic	LBBB

Summary of 24-hour Holter findings from patient clinical records.

LBBB: Left bundle branch block morphology
RBBB: Right bundle branch block morphology

Supplemental Table S2.4: ARVC–Control Group Comparisons

	Control			ARVC				
Parameter	**Median**	**Q1**	**Q3**	**Median**	**Q1**	**Q3**	**P**	**Significance**
Total Activation Time (msec)	42	36	47	52	44	64	0.007	**
Total Recovery Time (msec)	134	126	152	129	120	146	0.273	
Mean Epicardial ARI (msec, Fridericia Rate-Correction)	241	230	262	275	237	300	0.014	*
Mean Epicardial EGM Amplitude (mV)	2.28	2.00	3.03	2.58	1.69	2.96	0.735	
Mean Deflections Per-Electrogram	1.06	1.03	1.06	1.09	1.03	1.18	0.086	
Mean Epicardial Activation Time Gradient (ms/mm)	0.24	0.21	0.28	0.31	0.26	0.37	0.018	*
Mean Epicardial Recovery Time Gradient (ms/mm)	1.06	0.95	1.22	0.93	0.85	1.05	0.060	
Mean Epicardial ARI Gradient (msec, Fridericia Rate-Correction)	1.17	1.07	1.38	1.21	1.05	1.48	1.000	

Median, quartiles, and Wilcoxon rank sum comparison of ECGI EP parameters in healthy adults (Controls) and ARVC patients. Highlighted rows (yellow) indicate statistically significant differences between Control and ARVC groups.

Significance levels:
*** $p < 0.001$
** $p < 0.01$
* $p < 0.05$

Q1: First Quartile
Q3: Third Quartile

Supplemental Table S2.5: Mean Fridericia-Corrected Epicardial ARI (msec) in Controls and ARVC Patients with and without T-Wave Inversion

Controls					ARVC: T-Wave Inversion					ARVC: No T-Wave Inversion				
Median	Q1	Q3	Min	Max	Median	Q1	Q3	Min	Max	Median	Q1	Q3	Min	Max
241	230	262	206	274	300	269	313	218	330	238	231	262	226	285

Median, quartiles, Range, and Wilcoxon rank sum comparison of resting ARI (Fridericia rate-correction applied) in Controls and ARVC patients with and without T-Wave Inversion. Group difference ARVC with T-Wave Inversion is significantly different than controls at $p < 0.001$ level and ARVC without T-Wave Inversion at $p < 0.01$ level.

Q1: First Quartile
Q3: Third Quartile
Min: Minimum value observed in group
Max: Maximum value observed in group

Supplemental Table S2.6: Exercise Changes in ARVC Parameters

	Resting HR			Elevated HR				
Parameter	**Median**	**Q1**	**Q3**	**Median**	**Q1**	**Q3**	**P**	**Significance**
Total Activation Time (msec)	53	46	66	57	47	66	0.658	
Total Recovery Time (msec)	130	120	150	106	91	120	0.002	**
Mean Epicardial ARI (msec, uncorrected for HR)	275	235	313	186	173	203	< 0.001	***
Mean Epicardial EGM Amplitude (mV)	2.57	1.60	2.94	2.08	1.28	2.50	< 0.001	***
Mean Deflections Per-Electrogram	1.09	1.03	1.18	1.09	1.05	1.22	0.872	
Mean Epicardial Activation Time Gradient (ms/mm)	0.33	0.26	0.38	0.30	0.27	0.35	0.260	
Mean Epicardial Recovery Time Gradient (ms/mm)	0.94	0.87	1.06	0.70	0.60	0.88	0.007	**
Mean Epicardial ARI Gradient (msec, Fridericia Rate-Correction)	1.22	1.07	1.49	1.12	1.01	1.38	0.687	

Median, quartiles, and Wilcoxon signed-rank comparison of ECGI EP parameters in ARVC patients at Resting HR and Elevated HR after exercise. Highlighted rows (yellow) indicate statistically significant differences between Control and ARVC groups.

Significance levels:
*** $p < 0.001$
** $p < 0.01$
* $p < 0.05$

Q1: First Quartile
Q3: Third Quartile

Supplemental Table S2.7: Correlation of EP Substrate to LV Late Gadolinium Enhancement

Parameter	CC	P	Significance
EGM Amplitude	-0.42	< 0.001	***
Deflections Per-EGM	0.52	< 0.001	***
AT Spatial Gradient	0.24	0.001	**
Resting ARI	0.29	< 0.001	***
Exercise ARI	0.10	0.190	
RT Spatial Gradient	-0.09	0.232	
ARI Spatial Gradient	0.05	0.485	
Exercise ARI Shortening	0.31	< 0.001	***

Spearman correlation coefficients of LV LGE and EP substrate parameters. Highlighted rows (yellow) indicate statistically significant correlations between LV LGE and EP substrate parameters.

Significance levels:
*** $p < 0.001$
** $p < 0.01$
* $p < 0.05$

Supplemental Table S2.8: Correlation of EP Substrate to RV Late Gadolinium Enhancement

Parameter	CC	P	Significance
EGM Amplitude	-0.02	0.755	
Deflections Per-EGM	-0.05	0.472	
AT Spatial Gradient	-0.15	0.051	
Resting ARI	0.30	< 0.001	***
Exercise ARI	0.17	0.027	*
RT Spatial Gradient	-0.05	0.502	
ARI Spatial Gradient	-0.10	0.197	
Exercise ARI Shortening	0.36	< 0.001	***

Spearman correlation coefficients of RV LGE and EP substrate parameters. Highlighted rows (yellow) indicate statistically significant correlations between RV LGE and EP substrate parameters.

Significance levels:
*** $p < 0.001$
** $p < 0.01$
* $p < 0.05$

Supplemental Table S2.9: Correlation of LGE and EP Substrate with Regional Rate of Ventricular Ectopy

Parameter	CC	P	Significance
EGM Amplitude	-0.21	< 0.001	***
Deflections Per-EGM	0.20	< 0.001	***
AT Spatial Gradient	0.04	0.457	
Resting ARI	0.35	< 0.001	***
Exercise ARI	0.28	< 0.001	***
RT Spatial Gradient	-0.06	0.232	
ARI Spatial Gradient	0.00	0.943	
Exercise ARI Shortening	0.30	< 0.001	***
LV LGE	0.50	< 0.001	***
RV LGE	0.35	< 0.001	***

Spearman correlation coefficients of PVC rate within anatomical regions and EP substrate parameters and LGE. Highlighted rows (yellow) indicate statistically significant correlations between PVC Rate and substrate parameters.

Significance levels:
*** $p < 0.001$
** $p < 0.01$
* $p < 0.05$

Supplemental References (ECGI Methodology)

1. Rudy Y, Ramanathan C, Ghosh S. Noninvasive Electrocardiographic Imaging: Methodology and Excitation of the Normal Human Heart. In: Cardiac Electrophysiology: From Cell to Bedside. 2009. p. 467–472.

2. Rudy Y, Burnes JE. Noninvasive Electrocardiographic Imaging. *Ann Noninvasive Electrocardiol*. 1999;4:340–359.

3. Rudy Y, Oster HS. The electrocardiographic inverse problem. *Critical reviews in biomedical engineering*. 1992;20:25–45.

4. Ghosh S, Rudy Y. Accuracy of quadratic versus linear interpolation in noninvasive Electrocardiographic Imaging (ECGI). *Annals of biomedical engineering*. 2005;33:1187–1201.

5. Wang Y, Rudy Y. Application of the method of fundamental solutions to potential-based inverse electrocardiography. *Annals of biomedical engineering*. 2006;34:1272–1288.

6. Ramanathan C, Jia P, Ghanem R, Calvetti D, Rudy Y. Noninvasive electrocardiographic imaging (ECGI): application of the generalized minimal residual (GMRes) method. *Annals of biomedical engineering*. 2003;31:981–994.

7. Ghosh S, Rudy Y. Application of L1-norm regularization to epicardial potential solution of the inverse electrocardiography problem. *Annals of biomedical engineering*. 2009;37:902–912.

Chapter 3: Excitation and Contraction of the Failing Heart in situ and Effects of Cardiac Resynchronization Therapy

Christopher Andrews (BS), Gautam K. Singh (MD), Brian P. Cupps (PhD), Michael K. Pasque (MD) and Yoram Rudy (PhD)

3.1 Abstract

Background: Cardiac resynchronization therapy (CRT) is an effective treatment for heart failure (HF) with benefits that include reverse remodeling of the HF phenotype. Despite the success of CRT, the rate of nonresponders remains around 30%. Many small studies showed promising results applying speckle tracking echocardiography (STE) strain imaging to patient selection, but larger studies showed no benefits over standard criteria. Improvements to CRT require a more complete understanding of the physiological changes of reverse remodeling and the relationship between electrical and mechanical measures of synchrony.

Methods: We imaged 20 healthy controls and imaged 30 CRT patients longitudinally using electrocardiographic imaging (ECGI, a method for noninvasive cardiac electrophysiology mapping) and STE. We computed dyssynchrony with each technique and compared their relative effectiveness for predicting response to CRT. We quantified CRT-induced remodeling of electrical and mechanical physiological parameters. We measured the electromechanical delay between activation and peak strain within LV segments. We additionally performed tagged MR imaging on the healthy controls to provide a high-resolution 3D maps of activation, contraction, and repolarization in healthy human hearts.

Results: The delay between mean lateral LV and RV electrical activation time, determined with ECGI, was the best predictor of beneficial reduction in LV end systolic volume and outperformed mechanical indices (Spearman's Rho: -0.722, $p < 0.001$). The mean electromechanical delay within anatomical segments was similar in controls and HF patients, however, the HF patients had greater dispersion of delay and the values were dependent on the

activation sequence. After 6 months of CRT, patients had increased contraction magnitudes in native rhythm compared to baseline pre-CRT (baseline: -8.55%, 6 months: -10.14%, p=0.008). CRT also prolonged native rhythm repolarization at the location of the LV pacing lead (baseline: 280 msec, 6 months: 306 msec, p=0.002).

Conclusions: ECGI-measured LV activation delay is an effective index for CRT patient selection. CRT causes persistent improvements in contractile function, but increases dispersion of repolarization, which could increase the risk of arrhythmias. Electromechanical delay dispersion and sequence-dependence indicate that the timing of peak strains in STE is influenced by mechanical factors such as opposing wall contractions in addition to the activation sequence.

3.2 Introduction

Heart failure (HF) is a progressive disease with high prevalence and high mortality that is a major contributor to healthcare costs [1]. HF is associated with adverse remodeling of the ventricular myocardium that includes chamber dilatation, slow conduction, decreased myocyte contraction amplitudes, and prolonged action potential durations [2-5]. Approximately 30% of HF patients have electrical dyssynchrony, apparent by a prolonged QRS duration on the ECG [6], an indication of dyssynchronous ventricular contraction. Prolonged QRS duration and left ventricular ejection fraction (LVEF) are inversely correlated, and HF patients with QRS prolongation have higher all-cause mortality and may have a higher incidence of sudden death than those with narrow QRS complexes [6].

Cardiac resynchronization therapy (CRT) improves the synchrony of ventricular contraction by bi-ventricular pacing the ventricles. CRT has dramatically improved clinical outcomes for HF

patients with prolonged QRS durations. Large clinical trials found that CRT improves patient quality of life, reduces HF-related hospitalizations, prolongs patient survival, and may reduce the risk of sudden cardiac death [7-10]. CRT may also partially correct some of the pathological abnormalities in HF, a process known as reverse remodeling. Animal studies found that CRT restored cellular action potential duration (APD) and Ca^{2+} transients to normal levels [11,12]. Despite the widely reported benefits of CRT, the rate of patients who do not respond to the therapy has been remarkably stable at around 30% [13].

Multiple attempts have been made to improve on patient selection criteria for CRT using various electrical and mechanical indices of dyssynchrony. Multiple small studies reported promising results applying 2D speckle tracking echocardiography (STE) to CRT patient selection. STE is an imaging technique which tracks the characteristic speckled patterns in echocardiographic images and computes deformation of the patterns to determine strain [14]. Despite many promising initial evaluations, the multicenter PROSPECT trial found that no echocardiographic measures of dyssynchrony improved patient selection for CRT, and the EchoCRT trial, which evaluated CRT in patients with mechanical dyssynchrony and a narrow QRS complex, was stopped for futility with the conclusion that CRT was possibly detrimental in that patient cohort [15,16].

The disappointing performance of STE in CRT patient selection is an indication of gaps in our understanding of the electromechanics of HF and CRT. A better understanding of the physiology underlying response and non-response to CRT may advance future attempts to improve the therapy. Basic science explorations of human cardiac electromechanics, such as whole-heart computer simulations of electromechanical activity, may also contribute to better understanding

of CRT. However, electromechanical data from non-diseased human hearts are currently lacking [17]. The present study combines STE with Electrocardiographic Imaging (ECGI; a noninvasive method for cardiac electrophysiology mapping) [18] to study the electromechanics of CRT in HF patients in situ. We imaged CRT patients longitudinally to determine baseline dyssynchrony, acute resynchronization, and reverse remodeling after 3 and 6 months of CRT pacing. We also collected ECGI and STE from a group of 20 healthy adult volunteers to serve as a control baseline for comparison. In this group, we also performed tagged MRI [19] to provide a complete three-dimensional data set of the normal electromechanical sequence of healthy adult hearts.

3.3 Methods

3.3.1 Patient Cohort

We enrolled 20 healthy adults and 30 HF patients undergoing CRT at Washington University in St. Louis. Healthy volunteer demographics are provided in **Supplemental Table S3.1**, and HF characteristics are provided in **Supplemental Table 3.2**. The study was approved by the Human Research Protection Office at Washington University in St. Louis. All participants provided written informed consent.

3.3.2 Electrocardiographic Imaging (ECGI)

The ECGI method, developed and validated in our laboratory, was described previously [20]. A schematic of the is presented in **Supplemental Figure S3.1**. Briefly, 256 uniformly distributed ECGs were simultaneously recorded from the torso using a portable recording system (ActiveTwo, BioSemi; The Netherlands). Patient-specific heart-torso geometries were obtained from CRT patients using a thoracic CT scan gated at 70% of the R-R interval while wearing the

recording electrodes. Heart-torso geometries of normal subjects (controls) were obtained using a navigated anatomic MRI sequence. In these subjects, recording electrodes were replaced with MRI-visible markers prior to the scan, for compatibility with MRI. The ECG recordings were combined with the heart-torso geometries to reconstruct unipolar epicardial electrograms noninvasively, using previously described methods [20]. Typically, 1000 electrograms were computed over the entire ventricular epicardium. Electrograms over the valve plane were excluded from further analysis.

3.3.3 Echocardiography

Echocardiography was performed using a commercially available ultrasound imaging system (Vivid 7, GE Healthcare, Milwaukee, WI). Longitudinal strain was assessed in standard 4-chamber, 3-chamber (apical long axis), and 2-chamber apical views. Images were obtained using the maximum framerate that allowed for viewing the entire left ventricle (LV) chamber, with a typical frame rate of 70 frames per second. Strain curves in each apical view were computed using vendor speckle-tracking software (EchoPAC, GE Healthcare, Milwaukee, WI). To minimize the effect of noise on the timing of the strain curves, 3 beats were processed for each view and averaged. LV volumes and ejection fractions were determined using Simpson's biplane method. Volumes and ejection fractions were also determined using the averaged values of 3 beats. In cases where the 2-chamber view could not be obtained (n = 5) the 4-chamber volume parameters were used. We defined echocardiographic response as a decrease in LV end systolic volume (LVESV) $\geq$ 15% and/or an increase in ejection fraction (EF) $\geq$ 5% at 6 month visit.

3.3.4 Tagged MRI

Tagged MR images were obtained and analyzed using previously described methods [21]. ECG-gated images were obtained in short-axis and long axis views for a complete cardiac cycle beginning at end-diastole. Short axis slices were obtained with 8mm spacing from the level of the mitral valve to the LV apex. Four long-axis image sets were obtained in radially oriented planes. Tissue tagging was performed on each image using a Spatial Modulation of Magnetization radiofrequency tagging preparation, followed by 2-D balanced steady-state free precession cine image acquisition. Tagged and non-tagged images were acquired during the same breath hold to ensure similar anatomic positioning between images. Typical imaging parameters were described previously [21].

The strain analysis has been described and validated [22]. Epicardial and endocardial wall boundaries of the LV were defined in both short and long axis non-tagged images. Tag lines were delineated using a semi-automated active contour algorithm. The attachment points of the basal RV free wall were used in conjunction with a geometric model of the LV to create in finite element model of the LV. Strain was measured based on the deformation of the tagged surfaces throughout the cardiac cycle. 3D displacements were calculated from the movement of intramural tag surface intersection points during systole. StressCheck software (ESRD, Inc. St Louis, MO) was used to fit the displacement data and provide a continuous description of the displacement throughout the LV. Strain values in circumferential and longitudinal directions were calculated from this fitting.

3.3.5 Longitudinal CRT Studies

The first images of CRT patients were obtained after device implant but prior to the onset of CRT pacing. This allowed us to determine the location of the pacing leads from the CT scan and image the patients prior to any CRT-induced remodeling. Patients were imaged in their native (un-paced) rhythm and at the onset of CRT pacing. Imaging was repeated in both paced and un-paced rhythms after 3 and 6 months of CRT pacing. To avoid the radiation exposure of additional CT scans during follow-up visits, the recording electrodes were placed in the same locations as on the initial visit using anatomical images from the initial scan to guide electrode placement.

3.3.6 Analysis

Segmentation

Analysis of each imaging modality was performed blinded to the results of the other modalities. The data were compared based on anatomical regions. The LV was segmented using a modified version of the American Heart Association 17-Segment Model. The standard apical segments were replaced with anterolateral, inferolateral, anteroseptal, and inferoseptal apical segments. For the ECGI analysis, the lateral right ventricle (RV)was segmented using the same convention as the lateral LV. Electrogram parameters for each region were computed using the mean value from all electrograms within the region.

Electrogram Analysis

Activation times were computed from electrograms as the time of steepest negative time-derivative of voltage ($-dV/dt_{max}$). Recovery times were computed as the steepest positive time-

derivative during the T wave (dV/dt_{max}) [23]. Activation-recovery intervals (ARIs, a surrogate for local APD) were computed as the difference between recovery time and activation time. ECGI-reconstructed ARI values have been validated against direct intraoperative epicardial mapping in humans (see online supplement of Zhang et al [24]). Electrogram fractionation was quantified using the number of downward deflections between the QRS onset and T wave onset. Electrograms with more than 2 deflections were considered "fractionated" deflections. ARIs and fractionation were compared across visits in native rhythm only, to avoid the impact of altered activation sequence on the indices. Parameters were computed at pacing sites by averaging values of the 10 electrograms closest to the pacing lead locations.

Dyssynchrony Indices

We measured electrical dyssynchrony from the 12-lead ECG using the QRS duration. We defined the QRS duration as the latest QRS end in any lead minus the earliest QRS onset in any lead. We note that this definition differs from some measurements which report the QRS duration as the maximum duration in any single lead. The total activation time was defined as the latest epicardial activation time minus the earliest. We evaluated electrical dyssynchrony in ECGI using two previously reported indices. The LV activation delay was defined as the mean activation time in mid and basal lateral LV segments minus the mean activation time in mid and basal lateral RV segments [25]. The LV activation dispersion was defined as the standard deviation of activation times within the LV [26].

We evaluated mechanical synchrony using analogous indices applied to the echocardiographic strain data. The mechanical delay was defined as the mean time of peak strain in mid and basal

lateral LV segments minus the mean time of peak strain in mid and basal septal segments. This index was only computed for patients with at least two adequately-tracked segments in both the lateral LV and the septum. The mechanical dispersion was defined as the standard deviation of contraction times within the LV. This index was only computed in patients where strain data could be obtained in all 3 apical views.

Temporal Alignment

ECGI and echocardiographic parameters were aligned temporally using the body surface ECG from corresponding lead locations. Maxima or minima from the QRS voltage or voltage derivatives were used to align the ECG traces. Tagged MRI data were aligned temporally with the echocardiographic strain using the time of peak strain for each modality.

Statistical Analysis

Comparisons between controls and the HF population were performed using Wilcoxon rank-sum tests. Changes due to acute and chronic CRT pacing were assessed using Wilcoxon signed-rank tests. Correlations between parameters and volumetric reverse remodeling were performed using Spearman correlation coefficients.

3.4 Results

3.4.1 Healthy Controls

The control population in this study was used to characterize normal sequences of activation and contraction, and to establish normal ranges of electromechanical parameters (medians and interquartile ranges of all control electrical and mechanical parameters are provided in **Supplemental Table S3.3**). The epicardial activation sequence in healthy adults is very

consistent in its overall pattern. In all patients, the anatomical segment of earliest activation was located between the lateral RV and the anterior wall in mid or basal regions. The median time between earliest and latest activation in controls was 42 msec, and the maximum value we observed in the control group was 58 msec. In all controls the LV delay parameter was greater than 0 (mean lateral LV activation was later than mean lateral RV activation) with a median value of 14 msec. The activation isochrone map of a representative control is presented in **Figure 3.1**.

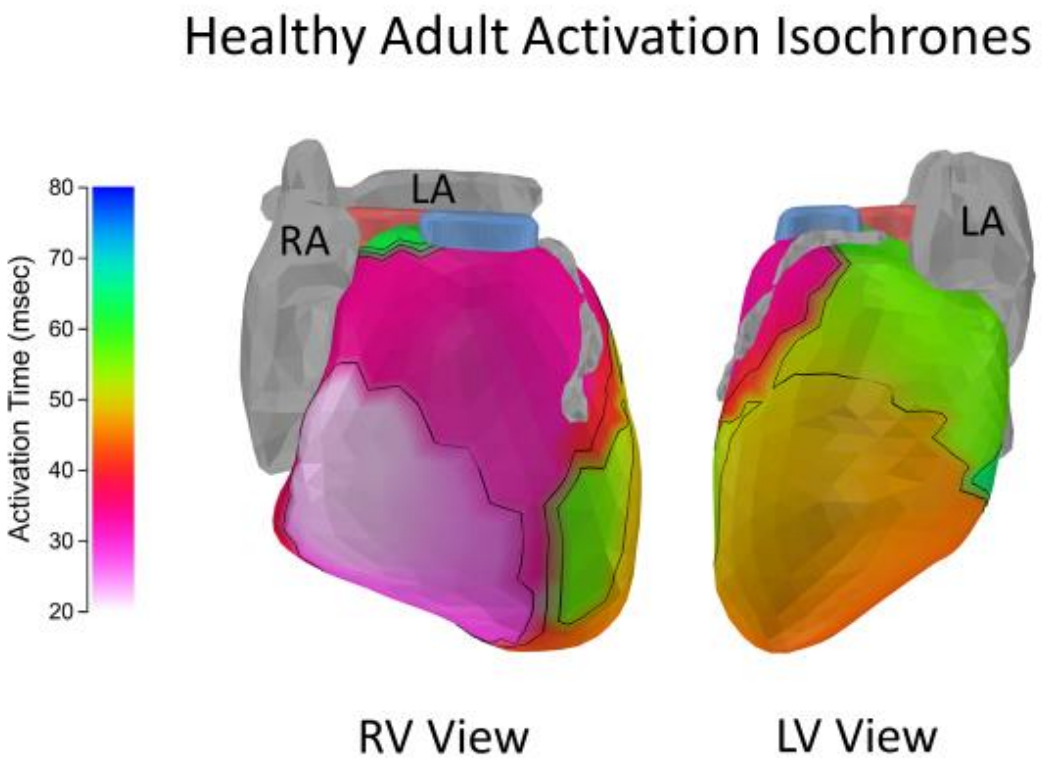

Figure 3.1. Activation isochrones in a healthy adult. Earliest activation in healthy adults falls between the lateral right ventricle (RV) and anterior wall. Atria and left anterior descending coronary artery are shown in gray. Right ventricular outflow tract shown in blue. Left ventricular outflow tract shown in pink. LV: left ventricle; RA: right atrium; LA: left atrium.

The sequence of LV strain in controls was similarly consistent. LV segments contractions were highly synchronous and reached peak strain approximately 430 msec after the onset of the QRS complex (medians and interquartile ranges for all control parameters are provided in **Supplemental Table S3.3**). The median mechanical delay was 12 msec, though there was more variability than in the electrical delay parameter and several subjects had negative values (peak septal strain after peak lateral LV strain). The mean delay between electrical activation and peak strain within anatomical segments was 375 msec. **Figure 3.2** presents the contraction sequence and mechanical parameters for a representative control. Combining tagged MRI with ECGI yields high resolution 3D maps of epicardial voltage and LV displacement and strain. An example of the 3D electromechanical sequence is presented in **Figure 3.2b**, and the **Supplemental Movie**.

Control repolarization was consistent with previous descriptions. The mean epicardial ARI value in the controls had a median value of 238 msec, which shows good agreement with the previously reported value of 235 msec [27]. The larger size of the control group in this study compared to the prior study allowed us to measure the difference in mean epicardial ARI between healthy male and female adults. Males had a median of 229 msec with 19 msec interquartile range, and females had a median of 261 msec with 23 msec interquartile range ($p = 0.001$). Representative ARI maps for a control male and a control female are presented in **Figure 3.3**.

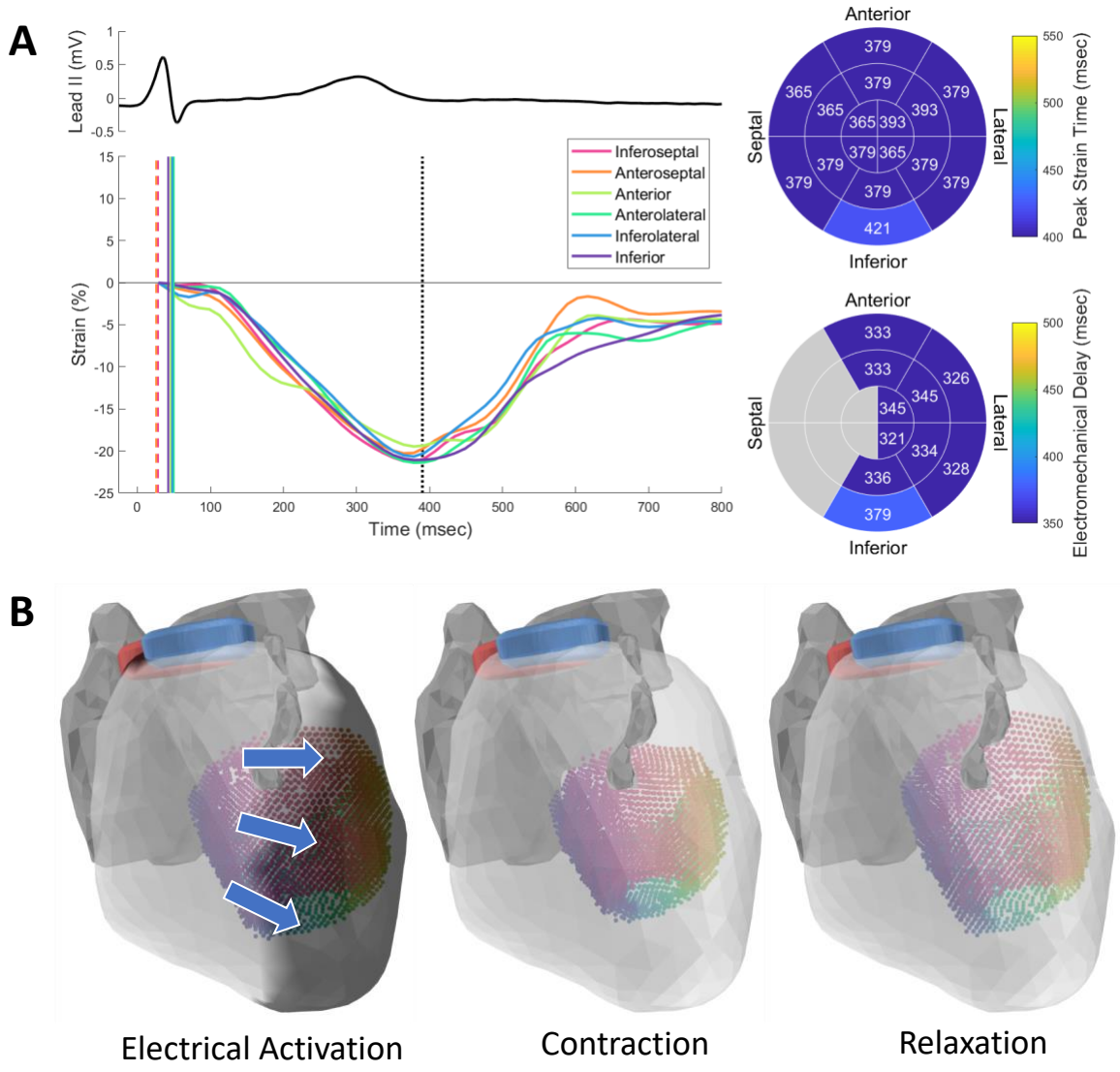

Figure 3.2. Healthy adult excitation and contraction. **A.** Speckle tracking echocardiography (STE) strain curves (top plot) plotted below the ECG. Electrical activation times are indicated in the plot with vertical lines (dashed lines indicate right ventricular activation as an approximation of septal activation time). Dotted line indicates aortic valve closure. The timing of peak strain within anatomical segments (top bullseye plot) was homogeneous within the LV. Regional electromechanical delay values (bottom bullseye plot) were computed by subtracting the electrical activation time from the time of peak strain within regions. **B.** Tagged MRI was performed on the controls, allowing for detailed electrical and mechanical imaging in the same coordinate system. Electrical activation is indicated as a transition from dark to light ventricular surface (left image). Tagged MRI displacement markers (colored dots; colors represent angular position within the LV) show the 3D contraction of the LV. An animation of the sequence is included in the **Supplemental Movie**.

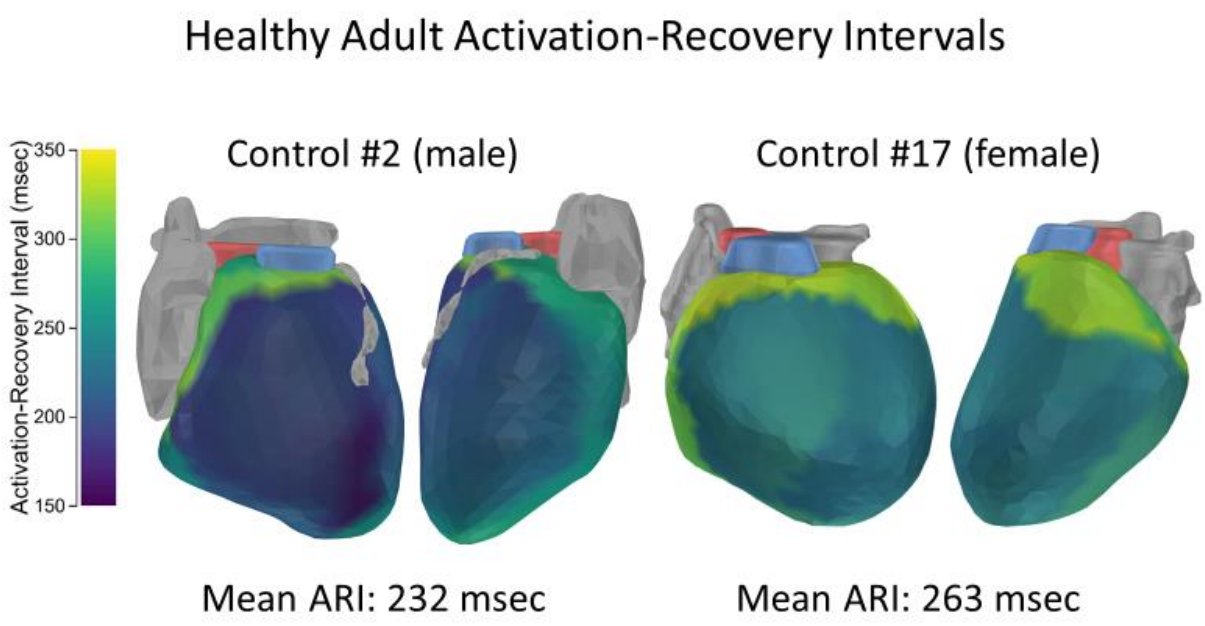

Figure 3.3 Activation-recovery interval (ARI) maps for a healthy adult male and female. Mean epicardial ARI values in female controls were approximately 30 msec longer than male controls. The longest ARI values were generally observed in the basal region.

3.4.2 Heart Failure and Cardiac Resynchronization Therapy

Electrical Activation

The native (un-paced) epicardial activation sequence in HF patients was prolonged compared to controls (statistical comparison to controls provided in **Supplemental Table S3.3**, changes due to acute CRT pacing onset provided in **Supplemental Table S3.4**). The most common pattern of epicardial activation in HF patients was characterized by a normal RV activation with varying degrees of delay in the lateral LV. In the majority of CRT patients, the primary factors in the efficacy of acute resynchronization were the baseline level of LV delay and the location of the

LV lead. **Figure 3.4** presents representative echocardiographic responders and nonresponders. The responders (patients 25 and 27) have high levels of baseline dyssynchrony with LV leads located in the region of late activation. The acute onset of CRT pacing resulted in significant improvement in the LV delay parameter. In contrast, the first nonresponder (patient 12) had a lower degree of baseline LV dyssynchrony, and the onset of pacing resulted in a smaller improvement in synchrony compared to the responders. The second nonresponder (patient 13) had a high degree of baseline dyssynchrony, however, the anterior location of this patient's lead reduced the effectiveness of pacing at synchronizing the ventricles.

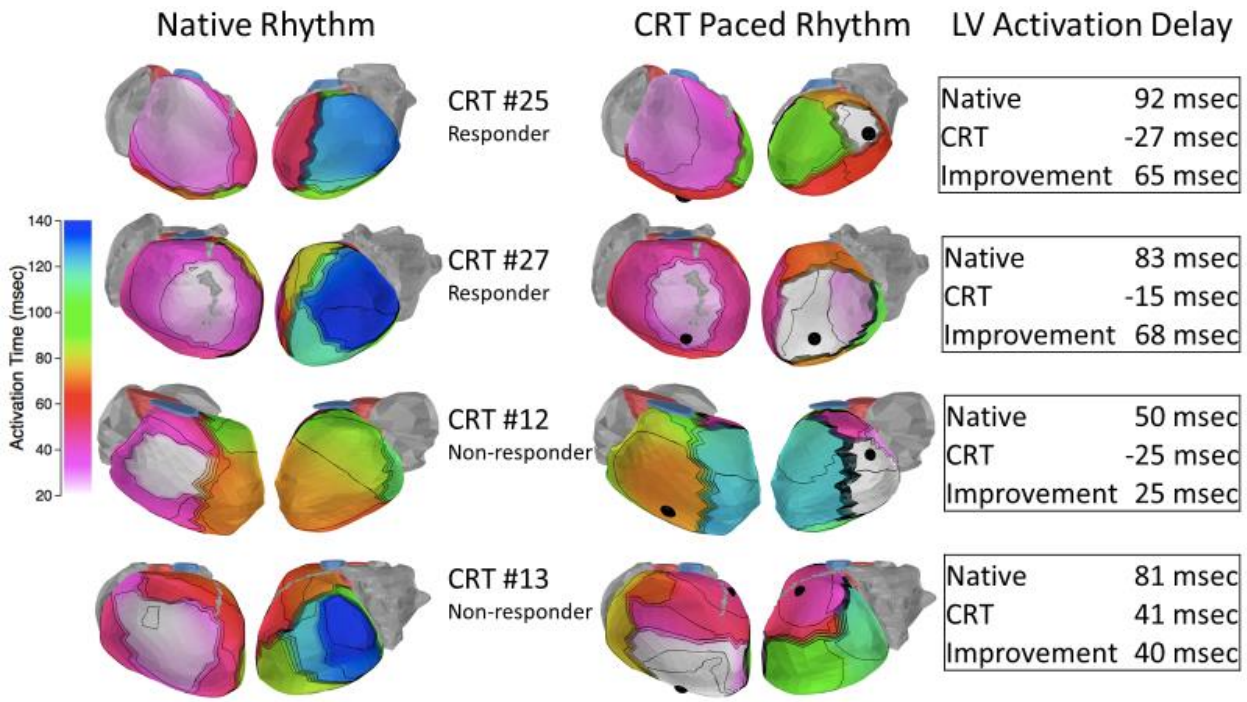

Figure 3.4 Activation isochrone maps in CRT patients in native rhythm prior to CRT pacing and at the onset of pacing. Pacing lead locations in the CRT-paced images are indicated with black spheres. LV activation delay values in each rhythm and the decrease in the absolute value of the index ("Improvement") are indicated to the right of the images. Echocardiographic responders (top 2 rows) generally had high levels of dyssynchrony at baseline, which was substantially improved by CRT pacing. Echocardiographic nonresponders often had less baseline dyssynchrony (row 3) or ineffective lead placement (row 4).

While baseline dyssynchrony and LV lead placement were major factors in acute resynchronization, the presence of scar affected the native rhythm and the efficacy of CRT pacing in several patients. Electrograms from regions of scar are characteristically low-amplitude and fractionated. By computing the number of steep downward deflections in electrograms we were able to quantify and visualize the electrophysiological substrate of scar. We found that HF patients had a higher percentage of fractionated electrograms than controls (median 1.77% in HF vs 0.38% in controls, $p = 0.001$). There were 5 patients with very high levels of epicardial fractionation (6 standard deviations above the control mean). Out of these 5 patients, 3 were nonischemic, 1 was ischemic, and 1 had mild nonosbstructive coronary artery disease. Three of these patients are presented in **Figure 3.5**.

Patient 10 (**Figure 3.5**, top row) demonstrates the impact that scar can have on the native activation sequence. The patient has a large lateral region of fractionation (left column), and the patient's native activation has a very long activation delay in the region of scar (middle column). The region of late activation is very small in this patient, and the onset of CRT pacing (right column) provides little to no improvement in synchrony. Patients 8 and 30 (**Figure 3.5**, middle and bottom rows, respectively) demonstrate the importance of lead placement in relation to scar. Patient 8 has an LV lead located in an inferolateral scar region, which resulted in delayed activation of the more anterior regions of the LV. Patient 30 had a region of scar in the basal lateral LV, but the patient's LV lead was located in the center of a region of healthy myocardium. This patient's synchrony improved substantially and the patient was an echocardiographic responder.

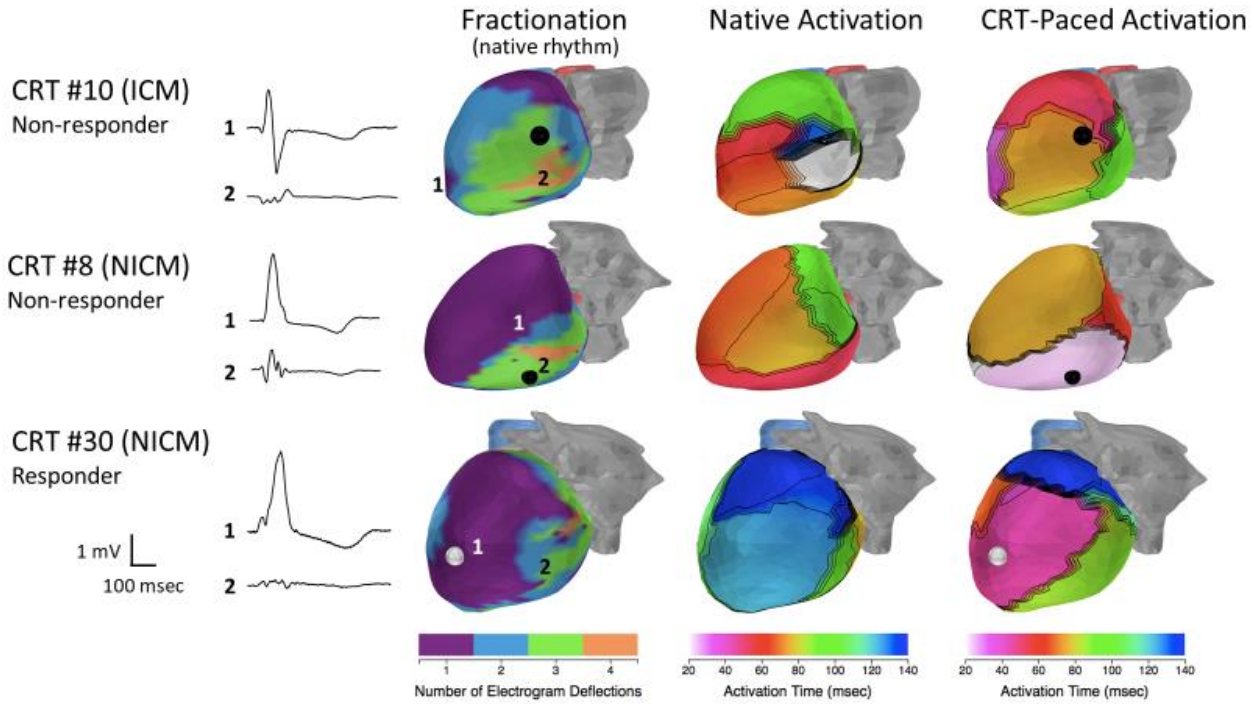

Figure 3.5 Maps of the number of deflections in each electrogram (first column), native rhythm activation (middle column), and CRT-paced activation (right column). Electrograms from the scar region and remote un-fractionated regions are provided to the left of the maps. Numbers indicate electrogram locations. Pacing electrode locations are indicated in the fractionation and CRT-paced activation maps with black or white spheres. Patients with high degrees of fractionation sometimes had atypical native rhythm activation sequences (top row). Pacing within regions of fractionation was less effective at activating nearby regions outside the scar (middle row). Patients with large regions of fractionation could still be resynchronized effectively when paced outside of the fractionated region (bottom row).

Contraction

Contraction in CRT patients was dyssynchronous and impaired. CRT patients had larger pre-systolic stretch and low peak contraction amplitudes than controls (full statistical comparisons presented in **Supplemental Table S3.3**). **Figure 3.6** (top) illustrates the native rhythm contraction sequence for a CRT patient. Electrical activation of the lateral LV is delayed relative to the other segments (vertical lines). The lateral LV was stretched by the septal wall contraction prior to its own contraction and the lateral wall segments reached peak contraction after aortic

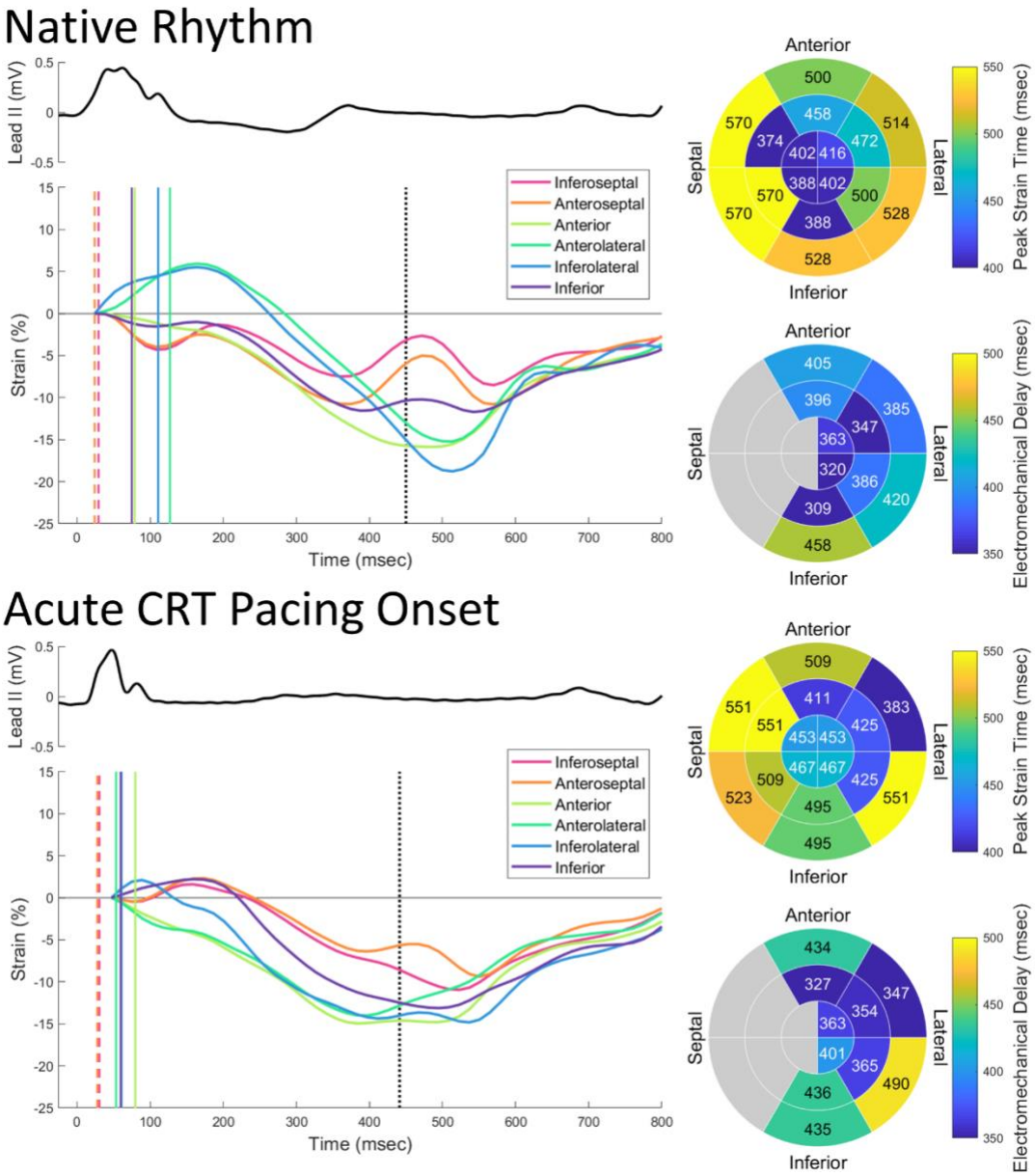

Figure 3.6. Native rhythm strains in heart failure (HF) patients (top) were dyssynchronous and lower in amplitude than controls. Lateral regions often stretched prior to contraction and reached peak strain after aortic valve closure (dotted line). Many regions were later to reach peak strain (top bullseye) than controls. The mean electromechanical delay in HF patients was the same as in controls, but the values within the LV showed greater dispersion (bottom bullseye). The Acute onset of CRT (bottom) decreased pre-systolic lateral wall stretch. Peak strain timing values did not capture synchrony improvements effectively. Regional electromechanical delay values were not consistent across different activation sequences.

valve closure (vertical dotted line). While the overall pattern of delayed LV contraction is apparent from the strain curves, it is difficult to extract meaningful markers of contraction timing from the plots because of the influence of opposing contraction and low amplitudes in some regions. In this patient, several of the septal wall segments reach peak strain after the lateral wall, despite the apparent overall pattern of delayed LV contraction. The mean electromechanical delays observed in HF patients closely matched control values, however, the dispersion of electromechanical delays within the LV were much larger.

The onset of CRT pacing improved the overall synchrony of the strain sequence (**Figure 3.6**, bottom). Lateral wall stretch is reduced, but peak strain values remained low compared to controls. The dispersion of electromechanical delay values in the LV was not corrected by the onset of CRT, and values within regions varied between the CRT and native rhythm. This indicates that the electromechanical delay cannot be regarded as an activation sequence-independent property of the underlying tissue.

Volumetric Reverse Remodeling

Of the 30 CRT patients, 22 patients completed the study and could be classified as echocardiographic responders or nonresponders. Out of these, 7 (32%) were nonresponders, consistent with the rate of nonresponders observed in most CRT studies. We used Spearman's rank correlation coefficient to correlate baseline native rhythm electrical and mechanical parameters with change in LVESV (**Supplemental Table S3.5**). In general, we found that electrical dyssynchrony parameters were much more predictive of reverse remodeling than mechanical dyssynchrony and function parameters. Each ECGI index of electrical dyssynchrony

(total activation time, LV electrical delay, and LV electrical dispersion) correlated with LVESV remodeling more strongly than QRS duration and all of the mechanical indices. The most predictive parameter was the LV electrical delay (rho = -0.722, $p < 0.001$). In addition to baseline parameters, we correlated improvements in synchrony parameters at the onset of CRT pacing with change in LVESV (**Supplemental Table S3.6**). In this evaluation, acute improvements to the LV activation delay and mechanical dispersion had the highest correlations with LVESV remodeling (rho = 0.679 and rho = 0.671, respectively). However, these correlations were both lower than the correlation between baseline LV delay and LVESV remodeling.

Electrical and Mechanical Remodeling

To assess changes in electrical and mechanical properties induced by chronic CRT pacing, we compared electrical and mechanical parameters in native rhythm prior to the onset of CRT pacing to native rhythm after 6 months of CRT. We found no significant changes in electrical or mechanical synchrony parameters when comparing native rhythm before and after chronic CRT pacing (**Supplemental Table S3.7**), indicating that the underlying level of dyssynchrony remains unchanged. Despite the unchanged native rhythm activation sequence, we found a persistent improvement in native rhythm contraction magnitudes after 6 months of CRT (Baseline median: -8.55%, Remodeled median: -10.14%, $p = 0.008$) and sustained EF improvement (Baseline median: 24%, Remodeled median: 27%, $p < 0.001$). **Figure 3.7** demonstrates the improved contraction in 4 CRT patients.

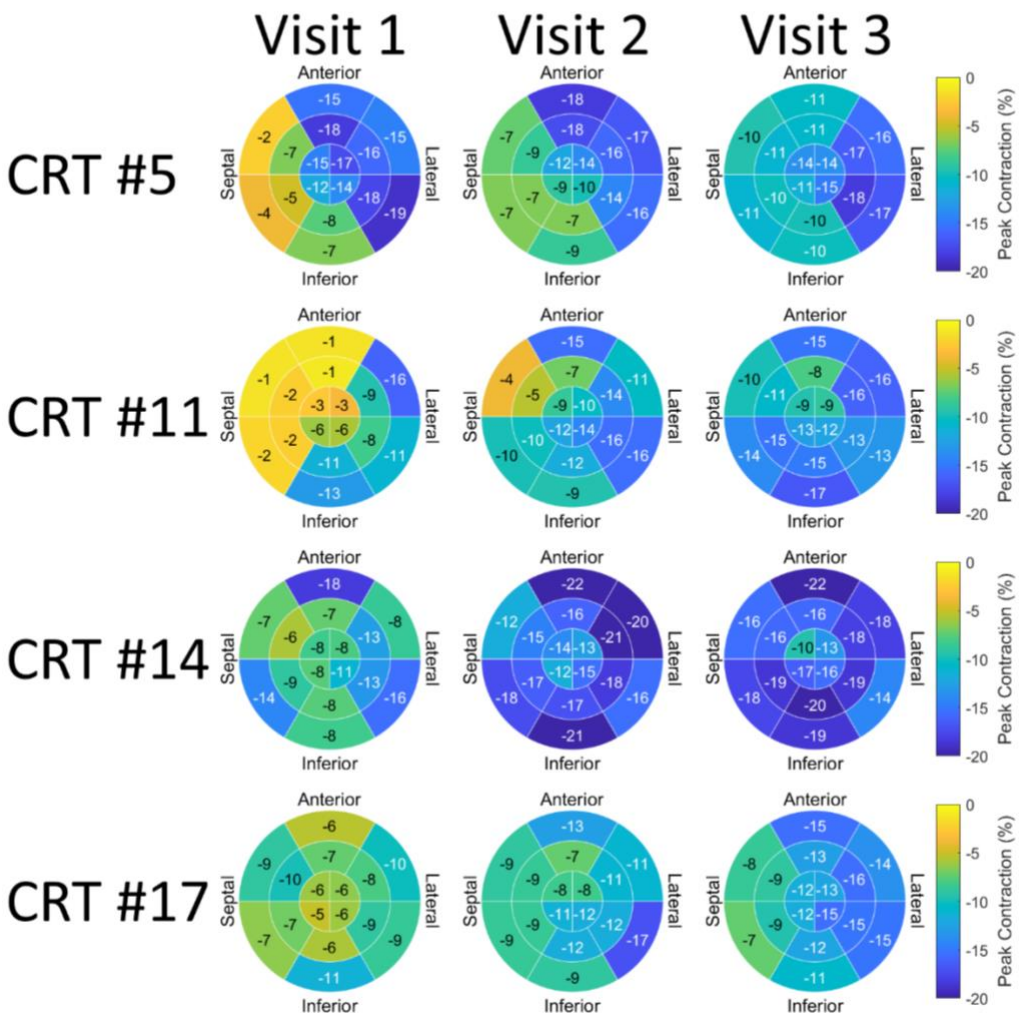

Figure 3.7 Peak contraction magnitudes are improved during the course of CRT. Values at each visit were determined from un-paced native rhythm beats, indicating persistent improvements in contraction as a result of chronic CRT pacing.

Prior to the onset of CRT, HF patients' mean epicardial ARIs were prolonged by about 45 msec compared to controls (**Supplemental Table S3.3**). After 6 months of CRT, mean epicardial

ARIs were largely unchanged (**Supplemental Table S3.7**). However, native rhythm ARIs near the LV pacing site were prolonged by a median value of 23 msec ($p = 0.002$). **Figure 3.8** presents baseline and remodeled ARI maps for 2 patients.

We correlated the changes in contraction and ARI prolongation at the LV pacing site with the change in ESV. The change in contraction was correlated with ESV change, but the LV ARI change was not (**Supplemental Table S3.8**). This suggests that the contraction improvement is part of the beneficial reverse remodeling changes induced by CRT, while the ARI prolongation is an effect of LV pacing that is not related to the beneficial reverse remodeling process.

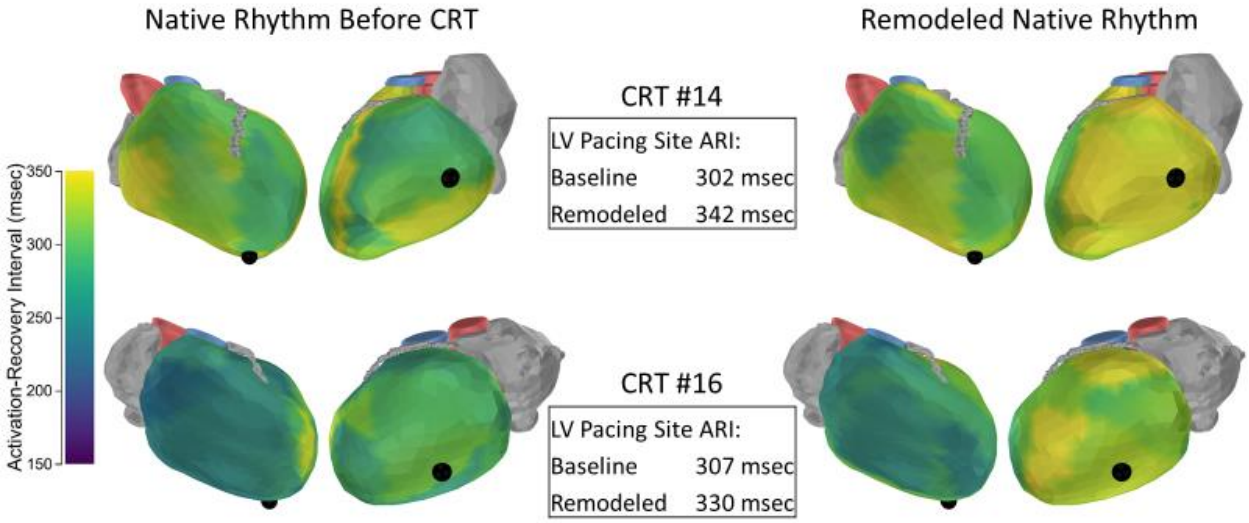

Figure 3.8. Epicardial activation-recovery interval (ARI) maps in heart failure (left) and after 6 months of CRT pacing (right). Heart failure patients had longer mean ARI values than control subjects at baseline. After 6 months of CRT pacing, ARI values were prolonged at the location of the left ventricle (LV) pacing lead.

3.5 Discussion

This paper presents the first combined application of ECGI and strain imaging in patients, thereby providing electrical and mechanical data from the same human hearts *in situ*. The following observations were made: 1. The LV electrical activation delay, determined from ECGI, outperforms mechanical measures of synchrony and is the best index for identifying potential responders to CRT. It also performs better than the QRS duration on the 12 – lead ECG that constitutes the standard of care in clinical practice. 2. Taking advantage of the panoramic mapping that ECGI provides, we discovered that LV pacing in CRT prolongs the APD in the region surrounding the electrode. The localization of the APD prolongation indicates that CRT pacing increases heterogeneity of repolarization, a known mechanism of arrhythmia. 3. We defined a novel parameter, the electromechanical delay between activation and peak strain within anatomical segments. We measured greater heterogeneity of the electromechanical delay in patients with dyssynchronous HF than controls. We also found that the electromechanical delay within regions is dependent upon the activation sequence. This implies that the timing of peak strains on echo does not merely reflect the electrical activation sequence, but is affected by the mechanics of opposing wall contractions. This may explain, in part, why STE has not seen greater success as a tool for CRT patient selection. 4. Through noninvasive assessment of healthy adult hearts, we demonstrated that the ARI on the epicardial surface in females is longer than males. Further study of gender-specific differences in repolarization with ECGI may help explain why women are more susceptible to arrhythmias associated with the long QT syndrome. 5. Using tagged MRI, we provide a high-resolution 3D description of contraction of healthy hearts that is co-registered spatially and temporally with detailed electrical activation and repolarization maps.

These data could be beneficial for constraining mathematical models and validating computer simulations of human cardiac electromechanics.

3.5.1 Control Physiology

The control population in this study is the largest group of healthy adults imaged with ECGI to date. This group served as a control for the current study and is valuable in that capacity as ECGI is applied to new pathologies. Additionally, the larger size of this study compared to a previous ECGI study of healthy adults allowed us to quantify the difference in epicardial repolarization between males and females. The longer repolarization we find in females is consistent with ECG findings that women have longer QTc intervals than men [28]. Exploring the link between this repolarization prolongation and the higher susceptibility of women to torsade de pointes would be an interesting application of ECGI [29].

The combination of ECGI, STE, and tagged MRI provide very detailed 3D characterizations of the healthy adult heart in situ. Tagged MRI provides detailed 3D displacement and strain data in the LV, however, the exact timing of the image acquisition relative to the ECG is opaque. By collecting STE, which is acquired with the body-surface ECG, in the same patients, we were able to align the strain curves temporally using the time of peak strain in each modality. The result is a detailed combination of electrical and mechanical sequences in healthy adult hearts. This data set may be particularly useful to constrain and validate mathematical models of the cardiac electromechanics.

3.5.2 Response to CRT

The initial evaluations of ECGI in CRT patients were retrospective studies of ischemic and nonischemic patients [25,26]. These studies evaluated two dyssynchrony indices: the LV activation delay and the LV activation dispersion. In the present prospective evaluation of electrical dyssynchrony and response to CRT, we found that both indices out-performed the body-surface ECG and mechanical indices, and that the LV delay index was the best predictor of volumetric reverse remodeling (**Supplemental Table S3.5**). That is, high level of inter-ventricular dyssynchrony, as measured by ECGI, is a good predictor of response to CRT. This is in agreement with a prior prospective ECGI study of CRT patients that found the LV delay (referred to in that study as ventricular electrical uncoupling) was superior to QRS duration at identifying responders [30]. A recent torso-tank study has directly validated ECGI reconstructions of this index compared to direct epicardial measurements [31]. In this study, we found that baseline electrical dyssynchrony was more correlated with LVESV remodeling than the improvement of synchrony at pacing onset. However, it would be valuable to explore whether using ECGI interactively to optimize lead placement and pacing timing would offer patients additional benefits.

An evaluation of ECGI in patients with pediatric congenital heart disease found that placing the LV lead in the site of latest activation resulted in favorable outcomes [32]. The present study demonstrated the ability of ECGI to image electrophysiological scar and showed its influence on dyssynchrony and pacing efficacy. Prior studies, using other imaging modalities, have demonstrated the importance of scar and its location relative to pacing leads for predicting CRT response [33]. However, ECGI offers the unique possibility of quantifying baseline dyssynchrony

with indices that may outperform the current standard of practice, identifying regions of delayed activation, imaging myocardial scar substrate, and evaluating the efficacy of lead location and other pacing parameters with a single imaging modality in real-time.

3.5.3 Remodeling

We found that contraction magnitudes increased as part of the CRT reverse remodeling process, and that the increased magnitudes persisted when comparing patients' baseline native rhythm to their native rhythm after 6 months of CRT. This, coupled with the absence of any activation sequence changes, indicates that the increased contraction was due to mechanical improvements. Cellular studies report decreased contraction amplitudes in myocytes isolated from failing human hearts [2]. Animal studies have reported that CRT restores intracellular Ca2+ transients to normal levels, which could improve contraction [11]. However, Ca2+ transient changes were associated with a reversal of APD prolongation [11,12], which we did not observe. Another possible mechanism for increase in contraction amplitudes is that they are secondary to the volumetric reverse remodeling. In simplified models, ventricular wall stress is proportional to chamber diameter as governed by the Law of Laplace [34]. The strong correlation between LVESV decrease and contraction amplitude supports this as a possible mechanism.

Multiple animal studies demonstrated ARI shortening as a result of CRT induced reverse remodeling [11,12]. In our study, we find not only that mean epicardial and mean LV ARIs do not decrease, but that at the site of the LV pacing lead native-rhythm ARIs increase by a median value of 23 msec. The discrepancy between our observations and the animal studies could be due to the

species differences, or the nature of the heart failure model, which was induced by RV tachypacing over a period of weeks to months.

The ARI prolongation we observed was not strongly correlated with LVESV, suggesting that it may be an effect of the pacing, rather than the reverse remodeling process. Prior work showed that pre-excitation due to RV pacing and Wolff-Parkinson-White syndrome were both associated with prolonged ARI in the region of pre-excitation [35,36]. In the present study, we observed ARI prolongation at the LV pacing site, but not the RV pacing site. It is noteworthy that CRT devices are often programmed so that the RV is activated by the intrinsic conduction system (illustrated in **Figure 3.4**, patients 25 and 27). This may cause less consistent pre-excitation at the RV lead location than the LV location and consequently a minimal effect on ARI.

There have been conflicting reports about whether CRT reduces or increases the risk of arrhythmia [10,37]. The finding of increased dispersion of repolarization due to ARI prolongation in the region of pacing suggests a mechanism for CRT increasing the risk of arrhythmia. The actual influence of this mechanism in the context of beneficial remodeling is unclear, however, this mechanism may be more significant in nonresponders. Because the ARI prolongation appears to be caused by the LV pacing and not reverse remodeling, nonresponders may be subjected to increased heterogeneity in repolarization without the benefits of improved LV function, which may be detrimental to their overall health. This underscores the importance of clinical criteria that properly exclude patients who will not benefit from CRT from receiving the treatment. Given these observations, it would be interesting to explore whether emerging LV pacing techniques such as

LV endocardial pacing, which may carry additional benefits [38], have a more favorable effect on repolarization.

3.5.4 Conclusion

The data support the utility of ECGI for improving patient selection for CRT. The timing of peak strain in STE is not a reliable index of local activation time when dyssynchrony is present. CRT-induced reverse remodeling improves contraction but prolongs repolarization at the LV pacing site, augmenting dispersion of repolarization. Additional studies are necessary to determine whether electrogram fractionation maps or interactive ECGI device optimization offer additional benefits to CRT treatment of HF patients.

Chapter 3 References

1. Benjamin EJ, Virani SS, Callaway CW, Chamberlain AM, Chang AR, Cheng S, Chiuve SE, Cushman M, Delling FN, Deo R, de Ferranti SD, Ferguson JF, Fornage M, Gillespie C, Isasi CR, Jiménez MC, Jordan LC, Judd SE, Lackland D, Lichtman JH, Lisabeth L, Liu S, Longenecker CT, Lutsey PL, Mackey JS, Matchar DB, Matsushita K, Mussolino ME, Nasir K, O'Flaherty M, Palaniappan LP, Pandey A, Pandey DK, Reeves MJ, Ritchey MD, Rodriguez CJ, Roth GA, Rosamond WD, Sampson UKA, Satou GM, Shah SH, Spartano NL, Tirschwell DL, Tsao CW, Voeks JH, Willey JZ, Wilkins JT, Wu JH, Alger HM, Wong SS, Muntner P. Heart Disease and Stroke Statistics—2018 Update: A Report From the American Heart Association. *Circulation*. 2018;137:e67–e492.

2. Davies CH, Davia K, Bennett JG, Pepper JR, Poole-Wilson PA, Harding SE. Reduced contraction and altered frequency response of isolated ventricular myocytes from patients with heart failure. *Circulation*. 1995;92:2540–2549.

3. Nattel S, Maguy A, Le Bouter S, Yeh Y-H. Arrhythmogenic ion-channel remodeling in the heart: heart failure, myocardial infarction, and atrial fibrillation. *Physiol Rev*. 2007;87:425–456.

4. Eapen Z, Rogers JG. Strategies to attenuate pathological remodeling in heart failure. *Curr Opin Cardiol*. 2009;24:223–229.

5. Tomaselli GF, Zipes DP. What causes sudden death in heart failure? *Circ Res*. 2004;95:754–763.

6. Kashani A, Barold SS. Significance of QRS complex duration in patients with heart failure. *J Am Coll Cardiol*. 2005;46:2183–2192.

7. Cleland JGF, Daubert J-C, Erdmann E, Freemantle N, Gras D, Kappenberger L, Tavazzi L, Cardiac Resynchronization-Heart Failure CARE-HF Study Investigators. The effect of cardiac resynchronization on morbidity and mortality in heart failure. *N Engl J Med*. 2005;352:1539–1549.

8. Abraham WT, Fisher WG, Smith AL, DeLurgio DB, Leon AR, Loh E, Kocovic DZ, Packer M, Clavell AL, Hayes DL, Ellestad M, Trupp RJ, Underwood J, Pickering F, Truex C, McAtee P, Messenger J, MIRACLE Study Group Multicenter InSync Randomized Clinical Evaluation. Cardiac resynchronization in chronic heart failure. *N Engl J Med*. 2002;346:1845–1853.

9. Bristow MR, Saxon LA, Boehmer J, Krueger S, Kass DA, de Marco T, Carson P, DiCarlo L, DeMets D, White BG, DeVries DW, Feldman AM, Comparison of Medical Therapy Pacing and Defibrillation in Heart Failure COMPANION Investigators. Cardiac-resynchronization therapy with or without an implantable defibrillator in advanced chronic heart failure. *N Engl J Med*. 2004;350:2140–2150.

10. Cleland JGF, Daubert J-C, Erdmann E, Freemantle N, Gras D, Kappenberger L, Tavazzi L. Longer-term effects of cardiac resynchronization therapy on mortality in heart failure [the CArdiac REsynchronization-Heart Failure (CARE-HF) trial extension phase]. *European heart journal*. 2006;27:1928–1932.

11. Nishijima Y, Sridhar A, Viatchenko-Karpinski S, Shaw C, Bonagura JD, Abraham WT, Joshi MS, Bauer JA, Hamlin RL, Györke S, Feldman DS, Carnes CA. Chronic cardiac resynchronization therapy and reverse ventricular remodeling in a model of nonischemic cardiomyopathy. *Life Sci*. 2007;81:1152–1159.

12. Aiba T, Hesketh GG, Barth AS, Liu T, Daya S, Chakir K, Dimaano VL, Abraham TP, O'Rourke B, Akar FG, Kass DA, Tomaselli GF. Electrophysiological consequences of dyssynchronous heart failure and its restoration by resynchronization therapy. *Circulation*. 2009;119:1220–1230.

13. Daubert C, Behar N, Martins RP, Mabo P, Leclercq C. Avoiding non-responders to cardiac resynchronization therapy: a practical guide. *European heart journal*. 2016;32:ehw270.

14. Blessberger H, Binder T. Non-invasive imaging: Two dimensional speckle tracking echocardiography: basic principles. *Heart*. 2010;96:716–722.

15. Chung ES, Leon AR, Tavazzi L, Sun J-P, Nihoyannopoulos P, Merlino J, Abraham WT, Ghio S, Leclercq C, Bax JJ, Yu C-M, Gorcsan J, St John Sutton M, de Sutter J, Murillo J. Results of the Predictors of Response to CRT (PROSPECT) trial. *Circulation*. 2008;117:2608–2616.

16. Ruschitzka F, Abraham WT, Singh JP, Bax JJ, Borer JS, Brugada J, Dickstein K, Ford I, Gorcsan J III, Gras D, Krum H, Søgaard P, Holzmeister J. Cardiac-Resynchronization Therapy in Heart Failure with a Narrow QRS Complex. *N Engl J Med*. 2013;369:1395–1405.

17. Rudy Y, Ackerman MJ, Bers DM, Clancy CE, Houser SR, London B, McCulloch AD, Przywara DA, Rasmusson RL, Solaro RJ, Trayanova NA, van Wagoner DR, Varró A,

Weiss JN, Lathrop DA. Systems approach to understanding electromechanical activity in the human heart: a national heart, lung, and blood institute workshop summary. *Circulation*. 2008;118:1202–1211.

18. Ramanathan C, Jia P, Ghanem R, Calvetti D, Rudy Y. Noninvasive electrocardiographic imaging (ECGI): application of the generalized minimal residual (GMRes) method. *Annals of biomedical engineering*. 2003;31:981–994.

19. Young AA, Axel L, Dougherty L, Bogen DK, Parenteau CS. Validation of tagging with MR imaging to estimate material deformation. *Radiology*. 1993;188:101–108.

20. Ramanathan C, Ghanem RN, Jia P, Ryu K, Rudy Y. Noninvasive electrocardiographic imaging for cardiac electrophysiology and arrhythmia. *Nat Med*. 2004;10:422–428.

21. Lindman BR, Liu Q, Cupps BP, Woodard PK, Novak E, Vatterott AM, Koerner DJ, Kulshrestha K, Pasque MK. Heterogeneity of systolic dysfunction in patients with severe aortic stenosis and preserved ejection fraction. *J Card Surg*. 2017;32:454–461.

22. Cupps BP, Taggar AK, Reynolds LM, Lawton JS, Pasque MK. Regional myocardial contractile function: multiparametric strain mapping. *Interactive CardioVascular and Thoracic Surgery*. 2010;10:953–957.

23. Coronel R, de Bakker JMT, Wilms-Schopman FJG, Opthof T, Linnenbank AC, Belterman CN, Janse MJ. Monophasic action potentials and activation recovery intervals as measures of ventricular action potential duration: experimental evidence to resolve some controversies. *Heart Rhythm*. 2006;3:1043–1050.

24. Zhang J, Hocini M, Strom M, Cuculich PS, Cooper DH, Sacher F, Haïssaguerre M, Rudy Y. The Electrophysiological Substrate of Early Repolarization Syndrome. *J Am Coll Cardiol EP*. 2017;

25. Jia P, Ramanathan C, Ghanem RN, Ryu K, Varma N, Rudy Y. Electrocardiographic imaging of cardiac resynchronization therapy in heart failure: observation of variable electrophysiologic responses. *Heart Rhythm*. 2006;3:296–310.

26. Ghosh S, Silva JNA, Canham RM, Bowman TM, Zhang J, Rhee EK, Woodard PK, Rudy Y. Electrophysiological Substrate and Intraventricular LV Dyssynchrony in Non-ischemic Heart Failure Patients Undergoing Cardiac Resynchronization Therapy. *Heart Rhythm*. 2011;8:–699.

27. Ramanathan C, Jia P, Ghanem R, Ryu K, Rudy Y. Activation and repolarization of the

normal human heart under complete physiological conditions. *Proc Natl Acad Sci USA*. 2006;103:6309–6314.

28. Merri M, Benhorin J, Alberti M, Locati E, Moss AJ. Electrocardiographic quantitation of ventricular repolarization. *Circulation*. 1989;80:1301–1308.

29. Clinical and genetic determinants of torsade de pointes risk. *Circulation*. 2012;125:1684–1694.

30. Ploux S, Lumens J, Whinnett Z, Montaudon M, Strom M, Ramanathan C, Derval N, Zemmoura A, Denis A, De Guillebon M, Shah A, Hocini M, Jais P, Ritter P, Haïssaguerre M, Wilkoff BL, Bordachar P. Noninvasive electrocardiographic mapping to improve patient selection for cardiac resynchronization therapy: Beyond QRS duration and left bundle-branch block morphology. *J Am Coll Cardiol*. 2013;

31. Bear LR, Huntjens PR, Walton RD, Bernus O, Coronel R, Dubois R. Cardiac electrical dyssynchrony is accurately detected by noninvasive electrocardiographic imaging. *Heart Rhythm*. 2018;15:1058–1069.

32. Silva JNA, Ghosh S, Bowman TM, Rhee EK, Woodard PK, Rudy Y. Cardiac resynchronization therapy in pediatric congenital heart disease: insights from noninvasive electrocardiographic imaging. *Heart Rhythm*. 2009;6:1178–1185.

33. Scar burden by myocardial perfusion imaging predicts echocardiographic response to cardiac resynchronization therapy in ischemic cardiomyopathy. *American Heart Journal.* 2006;153:105–112.

34. Zhong L, Ghista DN, Tan RS. Left ventricular wall stress compendium. *Comput Methods Biomech Biomed Engin*. 2012;15:1015–1041.

35. Ghosh S, Rhee EK, Avari JN, Woodard PK, Rudy Y. Cardiac memory in patients with Wolff-Parkinson-White syndrome: noninvasive imaging of activation and repolarization before and after catheter ablation. *Circulation*. 2008;118:907–915.

36. Marrus SB, Andrews CM, Cooper DH, Faddis MN, Rudy Y. Repolarization Changes Underlying Long-Term Cardiac Memory Due to Right Ventricular Pacing: Noninvasive Mapping With Electrocardiographic Imaging. *Circulation Arrhythmia and electrophysiology*. 2012;5:773–781.

37. Lin G, Rea RF, Hammill SC, Hayes DL, Brady PA. Effect of cardiac resynchronisation therapy on occurrence of ventricular arrhythmia in patients with implantable cardioverter

defibrillators undergoing upgrade to cardiac resynchronisation therapy devices. *Heart*. 2008;94:186–190.

38. Strik M, Rademakers LM, van Deursen CJM, van Hunnik A, Kuiper M, Klersy C, Auricchio A, Prinzen FW. Endocardial Left Ventricular Pacing Improves Cardiac Resynchronization Therapy in Chronic Asynchronous Infarction and Heart Failure Models. *Circulation Arrhythmia and electrophysiology*. 2012;5:191–200.

Chapter 3 Appendix

Supplemental Table S3.1: Control Population

ID	Age	Sex	Race	Ethnicity
C1	27.8	M	Asian	Not Hispanic
C2	28.1	M	Caucasian	Not Hispanic
C3	28.3	M	Caucasian	Hispanic
C4	27.5	F	Caucasian	Not Hispanic
C5	27.6	M	Caucasian	Not Hispanic
C6	27.0	M	Caucasian	Not Hispanic
C7	31.9	M	Caucasian	Not Hispanic
C8	27.3	M	Caucasian	Not Hispanic
C9	29.4	F	Caucasian	Not Hispanic
C10	25.1	F	Caucasian	Not Hispanic
C11	24.9	M	African American	Not Hispanic
C12	49.0	F	Caucasian	Not Hispanic
C13	22.1	F	Caucasian	Not Hispanic
C14	35.5	M	Caucasian	Hispanic
C15	24.1	M	African American	Not Hispanic
C16	34.8	F	Asian	Not Hispanic
C17	24.4	F	Caucasian	Not Hispanic
C18	22.0	F	Caucasian	Not Hispanic
C19	53.7	F	Caucasian	Not Hispanic
C20	31.0	F	Caucasian	Not Hispanic

Healthy adult volunteer demographics.

Supplemental Table S3.2: CRT Population

ID	Age	Sex	Race	Ethnicity	Etiology
EM1	53.0	F	Caucasian	Not Hispanic	NICM
EM2	64.0	F	Caucasian	Not Hispanic	NICM
EM3	71.9	M	Caucasian	Not Hispanic	NICM
EM4	63.3	M	Caucasian	Not Hispanic	NICM
EM5	54.4	M	Caucasian	Not Hispanic	NICM
EM6	73.0	F	Caucasian	Not Hispanic	NICM
EM7	66.3	M	Caucasian	Not Hispanic	ICM
EM8	59.8	M	Caucasian	Not Hispanic	NICM
EM9	69.5	F	Caucasian	Not Hispanic	NICM
EM10	62.4	M	Caucasian	Not Hispanic	ICM
EM11	69.3	F	Caucasian	Not Hispanic	NICM
EM12	67.5	M	Caucasian	Not Hispanic	ICM
EM13	60.1	M	African American	Not Hispanic	ICM
EM14	54.5	F	Caucasian	Not Hispanic	NICM
EM15	77.6	M	Caucasian	Not Hispanic	ICM
EM16	64.0	F	Caucasian	Not Hispanic	NICM
EM17	52.5	M	Caucasian	Not Hispanic	NICM
EM18	78.7	F	Caucasian	Not Hispanic	ICM
EM19	74.7	F	Caucasian	Not Hispanic	NICM*
EM20	34.7	M	Caucasian	Not Hispanic	NICM
EM21	77.5	M	Caucasian	Not Hispanic	ICM
EM22	81.1	M	Caucasian	Not Hispanic	ICM
EM23	55.3	M	Caucasian	Not Hispanic	ICM
EM24	74.1	M	Caucasian	Not Hispanic	NICM
EM25	51.3	F	Caucasian	Not Hispanic	NICM
EM26	72.4	M	Caucasian	Not Hispanic	ICM
EM27	40.5	F	African American	Not Hispanic	NICM
EM28	62.4	M	Caucasian	Not Hispanic	NICM
EM29	61.4	M	African American	Not Hispanic	NICM
EM30	64.1	M	African American	Not Hispanic	NICM

Cardiac resynchronization therapy patient demographics. ICM: Ischemic Cardiomyopathy. NICM: Nonischemic cardiomyopathy

*Mild nonobstructive coronary artery disease

Supplemental Figure S3.1: ECGI Methodology

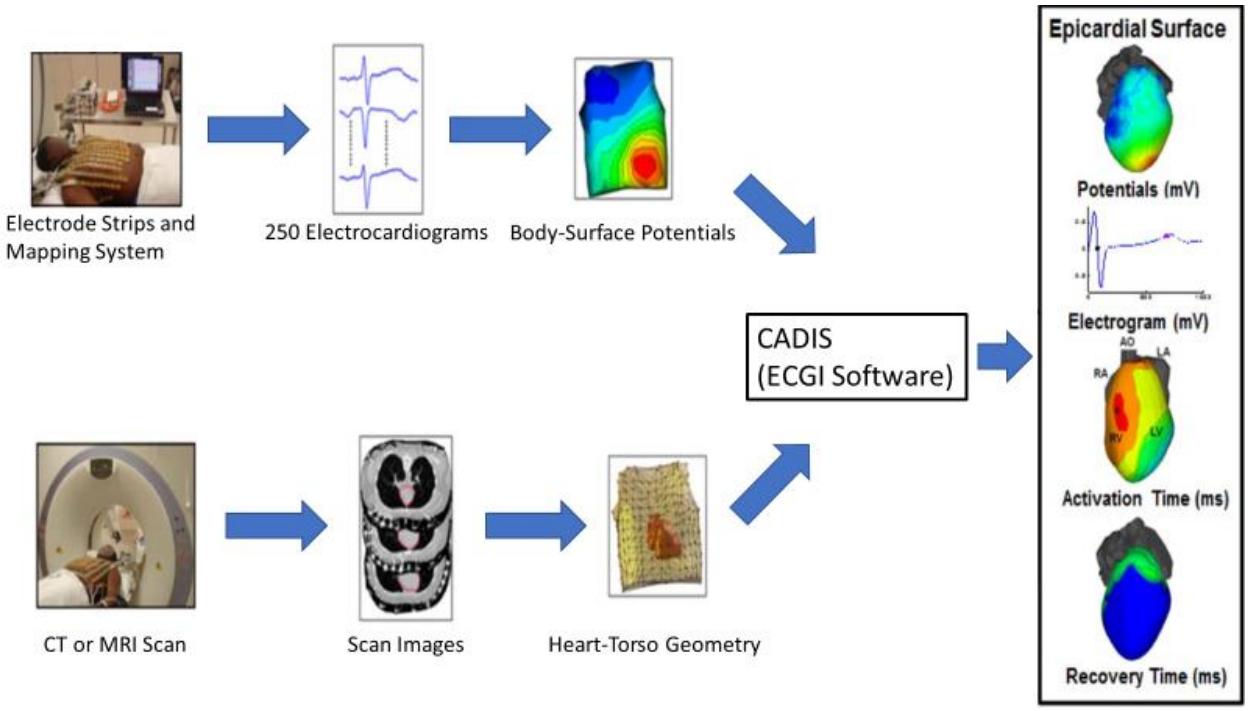

Schematic of the ECGI procedure. Body-surface potentials are recorded from the torso surface using a portable recording system (top). The heart-torso geometry is obtained using a computed tomography (CT) or magnetic resonance imaging (MRI) scan (bottom). The heart-torso geometry and torso potentials are combined and the inverse problem is solved to reconstruct unipolar epicardial electrograms. Electrograms are processed to determine local electrical parameters of interest (right frame).

Supplemental Table S3.3: Heart Failure Comparison to Controls

	Parameter	Control Median	Control IQR	Heart Failure Median	Heart Failure IQR	p
ECG	QRS duration (msec)	87	16	154	31	p < 0.001
Volume	Ejection fraction (%)	57	3	24	4	p < 0.001
	End systolic volume (mL)	46	20	122	56	p < 0.001
	End diastolic volume (mL)	111	36	160	72	0.002
	Stroke volume (mL)	63	18	39	19	p < 0.001
ECGI	Total activation time (msec)	42	12	123	33	p < 0.001
	LV activation delay (msec)	14	7	81	48	p < 0.001
	LV activation dispersion (msec)	9	3	24	9	p < 0.001
	Mean epicardial ARI (msec)	238	32	284	26	p < 0.001
	Mean LV ARI (msec)	240	23	292	25	p < 0.001
	Mean RV ARI (msec)	240	50	281	31	p < 0.001
	Percentage of fractionated electrograms (%)	0.38	1.03	1.77	2.11	0.001
	Fractionated deflections per electrogram	0.0038	0.0103	0.0179	0.0254	p < 0.001
Strain	Total strain time (msec)	98	42	196	67	p < 0.001
	Mechanical delay (msec)	12	53	91	112	p < 0.001
	Mechanical dispersion (msec)	28	10	70	19	p < 0.001
	Mean peak strain time (msec)	427	40	432	82	0.532
	Mean peak contraction (%)	-20.64	2.82	-8.78	2.42	p < 0.001
	Max pre-systolic stretch (%)	2.57	1.86	4.38	3.48	0.003
Electromechanical Delay	Mean electromechanical delay (msec)	375	40	373	50	0.940
	Electromechanical delay dispersion (msec)	25	15	57	19	p < 0.001

Control and heart failure baseline electrical and mechanical parameter comparison. All parameters were measured in native rhythm. Groups were compared using Wilcoxon rank-sum tests.

Supplemental Table S3.4: Acute Resynchronization

	Parameter	Native Median	Paced Median	Paired Delta Median	Paired Delta IQR	p
ECG	QRS duration (msec)	154	128	-37	31	p < 0.001
Volume	Ejection fraction (%)	24	27	3	4	p < 0.001
	End systolic volume (mL)	122	114	1	20	0.914
	End diastolic volume (mL)	160	168	5	29	0.094
	Stroke volume (mL)	39	43	7	9	p < 0.001
ECGI	Total activation time (msec)	123	104	-19	29	0.004
	LV activation delay (msec)	81	10	-62	53	p < 0.001
	LV activation dispersion (msec)	24	29	11	2	0.057
Strain	Total strain time (msec)	196	182	-14	75	0.223
	Mechanical delay (msec)	91	-15	-96	91	p < 0.001
	Mechanical dispersion (msec)	70	63	-9	40	0.046
	Mean peak contraction (%)	-8.78	-8.78	0.22	1.97	0.549
	Max pre-systolic stretch (%)	4.38	3.6	-1.23	2.19	0.009
Electromechanical Delay	Mean electromechanical delay (msec)	373	391	10	50	0.097
	Electromechanical delay dispersion (msec)	57	61	8	33	0.039

The effect of acute CRT pacing onset on electrical and mechanical parameters in heart failure patients. Changes were evaluated using Wilcoxon signed-rank tests.

Supplemental Table S3.5:

LVESV Remodeling Correlation with Baseline Parameters

	Parameter	Spearman's Rho	p
ECG	QRS duration (msec)	-0.486	0.023
ECGI	Total activation time (msec)	-0.583	0.005
	LV activation delay (msec)	-0.722	p < 0.001
	LV activation dispersion (msec)	-0.588	0.005
	Mean epicardial ARI (msec)	-0.110	0.625
	Mean LV ARI (msec)	0.168	0.454
	Mean RV ARI (msec)	-0.373	0.088
	Fractionated deflections per electrogram	0.241	0.280
	Fractionated deflections per electrogram at LV pacing site	0.387	0.075
Strain	Total peak strain time (msec)	-0.425	0.101
	Mechanical delay (msec)	0.132	0.639
	Mechanical dispersion (msec)	-0.585	0.019
	Mean peak contraction (%)	0.009	0.978
	Mean pre-systolic stretch (%)	-0.324	0.221
Electromechanical Delay	Activation-peak strain delay (msec)	-0.225	0.419
	Activation-peak strain delay spread (msec)	-0.204	0.466

Correlations between the change in left ventricular end-systolic volume (LVESV) after 6 months of CRT pacing and baseline electrical and mechanical parameters in heart failure patients. All parameters were measured in native rhythm. Correlations were determined using Spearman's Rho tests.

Supplemental Table S3.6:

LVESV Remodeling Correlation with Acute Dyssynchrony Index Changes

	Parameter	Spearman's Rho	p
ECG	QRS duration (msec)	0.505	0.017
Volume	Ejection fraction (%)	0.025	0.934
ECGI	Total activation time (msec)	0.407	0.061
	LV activation delay absolute value (msec)	0.679	p < 0.001
	LV activation dispersion (msec)	0.545	0.010
Strain	Total peak strain time (msec)	0.583	0.023
	Mechanical delay absolute value (msec)	0.013	0.965
	Mechanical dispersion (msec)	0.671	0.008

Correlations between the change in left ventricular end-systolic volume (LVESV) after 6 months of cardiac resynchronization therapy (CRT) pacing and the change in dyssynchrony parameters due to the acute onset of CRT pacing. Correlations were determined using Spearman's Rho tests.

Supplemental Table S3.7:

Native Rhythm Changes after 6 Months of CRT

	Parameter	Baseline Median	6 Months Median	Paired Delta Median	Delta IQR	p
ECG	QRS duration (msec)	154	157	5	11	0.164
Volume	Ejection fraction (%)	24	27	6	7	p < 0.001
	End systolic volume (mL)	125	121	-22	47	0.046
	End diastolic volume (mL)	167	171	-11	49	0.306
	Stroke volume (mL)	40	48	8	19	0.005
ECGI	Total activation time (msec)	123	115	-4	14	0.178
	LV activation delay (msec)	82	81	2	20	0.858
	LV activation dispersion (msec)	24	25	1	4	0.211
	Mean epicardial ARI (msec)	282	288	6	28	0.408
	Mean LV ARI (msec)	288	293	6	26	0.211
	Mean RV ARI (msec)	280	283	4	28	0.833
	LV pacing site ARI (msec)	280	306	23	36	0.002
	RV pacing site ARI (msec)	293	297	3	30	0.291
	Percentage of fractionated electrograms (%)	1.54	1.85	0.56	2.16	0.511
	Fractionated deflections per electrogram	0.0171	0.0235	0.0046	0.0492	0.565
Strain	Total peak strain time (msec)	196	210	14	77	0.891
	Mechanical delay (msec)	88	81	-6	65	1.000
	Mechanical dispersion (msec)	70	66	0	26	0.228
	Mean peak contraction (%)	-8.55	-10.14	-1.31	2.93	0.008
	Mean pre-systolic stretch (%)	4.59	3.48	-1.13	4.22	0.438
Electromechanical Delay	Activation-peak strain delay (msec)	367	381	14	45	0.169
	Activation-peak strain delay spread (msec)	57	50	-7	20	0.135

The effects of 6 months of cardiac resynchronization therapy pacing on heart failure patients' electrical and mechanical parameters. All parameters at each visit were computed from native rhythm beats. Changes were evaluated using Wilcoxon signed-rank tests.

Supplemental Table S3.8:

Correlation of LVESV Remodeling with ARI and Contraction Remodeling

Parameter	Spearman's Rho	p
LV pacing site ARI (msec)	-0.206	0.356
Mean peak contraction (%)	0.618	0.013

Correlation between the change in left ventricular end-systolic volume after 6 months of cardiac resynchronization therapy (CRT) pacing and the changes in ARI and contraction remodeling. Correlations were determined using Spearman's Rho tests.

Chapter 4: Concluding Remarks and Future Work

4.1 Concluding Remarks

This thesis demonstrated the utility of ECGI as a research and clinical tool by combining ECGI with complimentary imaging techniques to study new patient populations. The results of this work revealed new aspects of human heart physiology and point to roles for ECGI in the clinical care of patients.

The combination of ECGI and LGE imaging in ARVC patients revealed electrical abnormalities which co-localized with regions of visible scar. ARVC patients had abnormalities in conduction and repolarization. PVCs were common in ARVC patients, and they typically originated in regions of scar and electrical abnormalities. This finding implicates the electrical and structural abnormalities as mechanistic contributors to the formation of arrhythmia triggers in ARVC patients. In a young ARVC patient, we found that conduction abnormalities were visible before structural abnormalities. This suggests that the sensitivity of ECGI for detecting conduction abnormalities can play an important role in the early concealed phase of the disease.

By combining ECGI and strain imaging in CRT patients, we demonstrated that ECGI is effective for predicting response to CRT. The most sensitive index for predicting response to CRT was the LV activation delay determined by ECGI. STE indices were less effective predictors of response. The time delay between electrical activation and peak contraction within anatomical regions was variable and rhythm-dependent in CRT patients. This indicates that mechanical factors other than

the activation sequence influence the time of peak strain by STE. We showed that CRT pacing causes improvements in contraction that persist even when the pacing is temporarily disabled. We also found that CRT prolongs repolarization at the LV pacing site, which could increase the risk of arrhythmia.

4.2 Future Work

There are numerous opportunities for continuing to build upon this thesis and the work that preceded it. In the context of ARVC, this thesis demonstrated that ECGI detects electrical abnormalities in ARVC and linked them to PVCs, which can trigger dangerous arrhythmias. In order to relate the ECGI findings to the underlying scar substrate, the study used MRI-based LGE. A downside of using MRI to study patients with ARVC is that patients with ICDs were excluded from the study group because ICDs carry a contraindication for MRI. Because patients with a history of arrhythmia typically receive ICDs, the study population did not include any patients with a history of arrhythmia. Therefore, the study could not evaluate how predictive the various abnormalities were of arrhythmia. An important future study would be to compare patients with a history of arrhythmia to those without, and then determine whether any ECGI indices predict the risk of arrhythmia. Currently, the only widely accepted criterion for ICD implantation is a history of ventricular tachycardia. Because the first occurrence of ventricular tachycardia can be deadly, improved predictors of arrhythmia risk in ARVC patients are urgently needed.

A logical continuation of CRT research in this thesis would be to perform a larger prospective study to compare outcomes in patients selected for CRT by ECGI criteria to outcomes in patients

selected with conventional criteria. There are obvious benefits to delivering effective treatment to more patients. There are also benefits to accurately identifying patients who will not respond to the treatment. As the EchoCRT clinical trial showed, CRT may be detrimental in patients who do not need the treatment. Our data suggest that heterogenous repolarization may contribute to the detrimental effects of pacing these patients. Accurate identification of nonresponders could help decrease healthcare costs and direct more effective treatment strategies to nonresponders. Another avenue for exploration is using ECGI to optimize CRT pacing settings. The relative timing of pacing leads is an important factor in the overall effectiveness of pacing. Even modest improvements over current practices could have a very large impact because of the large population of heart failure patients.

There are many important applications outside of ARVC and CRT that should be further explored. One of the most interesting recent developments in the field of cardiac electrophysiology is the emergence of noninvasive ablation. Treatment for arrhythmia is traditionally performed in an invasive procedure in which a catheter is guided to the heart and used to burn regions of tissue that are responsible for starting or sustaining arrhythmia. A recent pilot study performed at Washington University in St. Louis tested the use of radiation therapy as an alternative to the standard invasive ablation procedure [1]. Noninvasive ablations were performed on 5 patients with ventricular tachycardia that was refractory to conventional treatment. Prior to ablation, the patients were mapped with ECGI, and ECGI maps were used to help guide the ablation target. The treatment resulted in a 99.9% reduction in ventricular tachycardia in the patient cohort. The combination of noninvasive electrical mapping and noninvasive ablation are a natural pairing, and evaluation of this approach is already underway in

a larger cohort. While the early results of this work are very exciting, there are many improvements that can be made. Improvements to the delivery of radiation should include incorporation of cardiac motion. Currently, the target is chosen for optimal delivery throughout the cardiac cycle, but unnecessary radiation delivery to healthy surrounding tissue could be reduced by incorporating cardiac motion. This thesis demonstrated that ECGI is compatible with tagged MRI, which tracks the motion of the left ventricle throughout the cardiac cycle. Beyond tagged MRI, the compatibility of ECGI with CT and MRI enables its combination with numerous other imaging techniques that could improve radiation delivery.

Finally, the ultimate success of any clinical tool depends on evidence-based guidelines for its application and its cost-effectiveness for improving patient outcomes. While ECGI was applied purely as a research tool in this work, the technique is now commercially available. In order to maximize the long-term benefits that ECGI can offer, future research must continue to prove the benefits of clinical ECGI, and commercial development must ensure that those benefits are cost-competitive within the context of current standards of practice.

Chapter 4 References

1. Cuculich PS, Schill MR, Kashani R, Mutic S, Lang A, Cooper D, Faddis M, Gleva M, Noheria A, Smith TW, Hallahan D, Rudy Y, Robinson CG. Noninvasive Cardiac Radiation for Ablation of Ventricular Tachycardia. *N Engl J Med*. 2017;377:2325–2336.